L-arginine ameliorates defective autophagy in GM2 gangliosidoses by mTOR modulation

Beatriz Castejón-Vega[1], Débora Lendines-Cordero[1], Alejandro Rubio[2], Antonio J. Pérez-Pulido[2], Pedro Bullón[1], José L. Quiles[3], Jon D. Lane[4], Beatriz Fernández Domínguez[5], María Begoña Cachón-González[6], Carmen Martín-Ruiz[7], Alberto Sanz[8], Timothy M. Cox[6], Elísabet Alcocer-Gómez[9], Mario D. Cordero[10]

[1] Research Laboratory, Oral Medicine Department, University of Sevilla, Sevilla, Spain

[2] Centro Andaluz de Biologia del Desarrollo (CABD, UPO-CSIC-JA). Facultad de Ciencias Experimentales (Área de Genética), Universidad Pablo de Olavide, 41013, Sevilla, Spain.

[3] Department of Physiology, Institute of Nutrition and Food Technology "José Mataix Verdú", Biomedical Research Center, University of Granada, Granada, Spain.

[4] Cell Biology Laboratories, School of Biochemistry, University of Bristol, Bristol, UK

[5]Acción y Cura para Tay-Sachs (ACTAYS), Madrid, Spain

[6] Department of Medicine, University of Cambridge, Cambridge, UK.

[7] Biosciences Institute, Newcastle University, Newcastle upon Tyne, UK.

[8]Institute of Molecular, Cell and Systems Biology, University of Glasgow, Glasgow G12 8QQ, UK.

[9] Departamento de Psicología Experimental, Facultad de Psicología, Universidad de Sevilla, Seville Spain.

[10] Instituto de Investigación e Innovación en Ciencias Biomédicas de Cádiz (INiBICA), Cadiz, Spain.

Emails: Beatriz Castejón-Vega1 beacastej92@outlook.es, Débora Lendines-Cordero1 deboralc93@gmail.com, Alejandro Rubio2 arubval@upo.es, Antonio J. Pérez-Pulido2 ajperez@upo.es, Pedro Bullón1 pbullon@us.es, José L. Quiles3, Jon D. Lane4 Jon.Lane@bristol.ac.uk, Beatriz Fernández Domínguez5 beatriz@actays.org, María Begoña Cachón-González6 mcb23@medschl.cam.ac.uk, Carmen Martín-Ruiz7 carmen.martin-ruiz@newcastle.ac.uk, Alberto Sanz8 Alberto.SanzMontero@glasgow.ac.uk, Timothy M. Cox6 tmc12@medschl.cam.ac.uk,

Elísabet Alcocer-Gómez9 ealcocer1@us.es, Mario D. Cordero10 mario.cordero@inibica.es

deboralc93@gmail.com

Running Title: Disrupted autophagy and mTOR in Tay-Sachs disease.

Corresponding Authors:

Dr. Mario D. Cordero
Instituto de Investigación e Innovación en Ciencias Biomédicas de Cádiz (INiBICA), Cadiz, Spain, Email: mario.cordero@inibica.es

Keywords: Tay-Sach, Sandhoff, autophagy, Lysosome, mTOR, Arginine

Tay-Sachs and Sandhoff diseases (GM2 gangliosidosis) are autosomal recessive disorders of lysosomal function that cause fatal and progressive neurodegeneration in infants and young children. Impaired hydrolysis catalysed by β-hexosaminidase A (HexA) leads to the accumulation of its specific substrate, GM2 ganglioside, in neuronal lysosomes. Despite the development of a florid storage phenotype, the role of autophagy and its regulation by the mammalian target of rapamycin (mTOR) has yet to be explored in the neuropathogenesis. Accordingly, we investigated the effects on autophagy and lysosomal integrity using skin fibroblasts obtained from patients with Tay-Sachs and Sandhoff diseases. Pathological autophagosomes, with enhanced expression of the p62/SQSTM1 protein, suggested impaired autophagic flux, an abnormality confirmed by electron microscopy and biochemical studies revealing the accelerated release of mature cathepsins and HexA into the cytosol, indicating increased lysosomal permeability. GM2 fibroblasts showed inappropriately diminished mTOR signalling with reduced basal mTOR activity. Accordingly, provision of a positive nutrient signal by L-arginine supplementation partially restored mTOR activity and ameliorated the cytopathological abnormalities - and immediately suggests an avenue for therapeutic exploration in this cruel disease. We also contend that the expression of autophagy/lysosome/mTOR-associated molecules may prove useful peripheral biomarkers for facile monitoring of systemic treatment of GM2 gangliosidosis and neurodegenerative disorders that affect the lysosomal function and disrupt autophagy

Keywords: Autophagy, mTOR; GM2 gangliosidosis; L-arginine

Autophagy is a degradation and clearance function of the lysosome that is critical for cellular homeostasis [1]. Where the digestive function is defective, as in the inherited Lysosomal Storage Disorders (LSD), accumulation of undegraded substrates in the lysosomal compartment can impair this fusion process [4]. As a result, in most of these genetic diseases, autophagic flux is arrested - with the consequential accumulation of other autophagy substrates including cell debris and organelles such as mitochondria, as well as the cargo protein, sequestosome-1 - also known as the ubiquitin-binding protein p62 (SQSTM1/p62) [3,4].

Autophagy is regulated by diverse mechanisms, each of which serves as a potential axis for therapeutic intervention. The mechanistic target of rapamycin (mTOR) is a highly conserved serine/threonine kinase that serves as a master regulator of metabolic processes centred on autophagic control. Moreover, the action of mTOR promotes lysosomal biogenesis and sustains the functional activity and integrity of this cell compartment [6]. Modulation of mTOR activity has been reported in Pompe disease, the first LSD to be biochemically characterised, where the significant muscular atrophy can be ameliorated by experimental induction of mTOR, which leads to substantial clearance of autophagic debris [7].

Here we have explored the role of autophagy in a class of lysosomal diseases - GM2 gangliosidosis Tay-Sachs and Sandhoff diseases - which principally affects sphingolipid recycling in the nervous system. The molecular cell pathology of these conditions reflects the striking accumulation of the primary substrate, GM2 ganglioside in neuronal lysosomes. That is due specifically to impaired hydrolysis *in situ* by β-hexosaminidase A (HexA). HexA is assembled as a functional heterodimer of α and β subunits. In humans, these proteins are encoded by *HEXA* and *HEXB* respectively, and the cognate subtypes are known as the genetically distinct, Tay-Sachs (Online Mendelian Inheritance in Man,

OMIM, #272800) or Sandhoff (OMIM # 268800) Diseases. Since the neurodegenerative features are clinically indistinguishable, diagnosis relies primarily on enzymatic assays selective for the different β-hexosaminidase isozymes A (α/β heterodimer; HexA); B (β/β homodimer; HexB) and S (α/α homodimer; HexS).

According to our study, we report that, when compared with healthy control cells, there is an enhanced expression of p62/SQSTM1 and build-up of autophagosomes, indicating impaired autophagic flux. This abnormality in fibroblasts from patients with GM2 gangliosidosis was confirmed by biochemical analysis and electron microscopy. Further, we observed an excess release of mature cathepsin B isoform and hexosaminidase A into the cytosol, which shows that lysosomal permeability is pathologically increased. GM2 fibroblasts had inappropriately diminished mTOR signalling with reduced basal mTOR activity. It is noteworthy that L-arginine supplementation of the diseased cells partially ameliorated these cytopathological abnormalities and immediately suggests an avenue for facile therapeutic exploration in this cruel disease.

MATERIAL AND METHODS

Ethical Statements

The work described was approved by the Ethics Committee of the Virgen de la Macarena and Virgen del Rocio University Hospitals, Seville, Spain, according to the principles of the Declaration of Helsinki and International Conferences on Harmonization and Good Clinical Practice Guidelines with the code 0795-N-15. All the participants in the study or their legal representatives gave written informed consent before the start of this study. Patients and samples were selected and isolated respectively from Hospital Clínico Santiago de Compostela (Dr Sánchez Pintos), Hospital 12 de Octubre (Dr Morales Conejo), Hospital La Fe de Valencia (Dr Pitarch Castellano), Hospital San Pedro de

Logroño (Dr García Oguiza), Hospital Niño Jesús de Madrid (Dr González Gutiérrez-Solana), Hospital Son Espases (Dr Inés Roncero). The suspected diagnosis of GM2 gangliosidosis had been made by specific tissue (skim biopsies) enzyme studies at the appropriate specialist reference centre (Centre de Diagnòstic Biomèdic, Hospital Clínic de Barcelona), and Tay-Sachs or Sandhoff diseases were confirmed by molecular analysis of the *HEXA* or *HEXB* genes, respectively. The clinical presentation and diagnostic information are presented in the supplementary tables (S1).

Fibroblast culture

Fibroblasts from patients with GM2 gangliosidosis were obtained from skin biopsy samples according to the Helsinki Declarations of 1964, as revised in 2001 for this specific research project according to the approved ethical committee 0795-N-15. Control fibroblasts were commercial primary dermal fibroblast from Juvenile and Infant donors (Primacyt Cell Culture Technology GmbH, Schwerin, Germany). Two-line of control fibroblasts were used and represented by the mean of both compared with the different patients. Fibroblasts were cultured in high glucose DMEM (Dulbecco's modified media) (Gibco, Invitrogen, Eugene, OR, USA). The medium was supplemented with 10% fetal bovine serum (FBS) (Gibco, Invitrogen, Eugene, OR, USA) and antibiotics (Sigma Chemical Co., St. Louis, MO, USA). Cells were incubated at 37ºC in a 5% CO_2 atmosphere. The medium was changed every two days to avoid changes in pH.

Statistical Analysis

Data in the figures is shown as mean ± SD. Data between different groups were analysed statistically by using ANOVA on Ranks with Sigma Plot and Sigma Stat statistical software (SPSS for Windows, 19, 2010, SPSS Inc. Chicago, IL, USA). For cell-culture studies, Student's t test was used for data analyses. A value of $p<0.05$ was considered significant.

Results

Mutant fibroblasts from Tay-Sachs patients showed impaired autophagic flux

Six patients, 3 infantile and 3 juvenile, contributed to this study. The clinical characteristics of these patients are included in supplementary Table 1. With the exception of juvenile patient 1 and infantile patient 3, the point mutations identified in the HEXA and HEXB genes were predicted to destabilise the intact protein. The latter, (allele 2), was especially noteworthy since the mutation was predicted to confer greater structural stability. However, the amino acid replacement directly affects the active site region. Patients 1 and 2 with the infantile-onset disease have non-coding mutations in close apposition to splice sites (Figure 1A-C and supplementary Table 2). Those mutations were considered to be the most destabilising and to have a more profound effect on hexosaminidase A catalysis as revealed by the impaired activities (compared with the reference values from healthy individuals (Figure 1D)).

Here we explore the cellular pathogenesis of GM2 gangliosidosis. In culture, the skin fibroblasts obtained from patients had impaired growth rates and markedly abnormal lysosomal morphology (Figure 1E and F). Western blotting studies showed increased abundance of the immunoreactive autophagy markers, LC3-II and p62/SQSTM1; the intracellular accumulation of lysosomal substrates as determined by p62/SQSTM1 was confirmed by immunofluorescence confocal microscopy (Figure 1G and H).

To investigate the integrity of lysosomal maturation and the formation of autophagosomes, we used bafilomycin A1 as an inhibitor of the vacuolar H^+ ATPase (vATPase). The bafilomycin A1 (BafA1) assay serves as a means to explore autophagosome/autophagolysosomal formation in the living cell. As expected, its effects on vATPase caused BafA1 to abrogate lysosomal acidification and intralysosomal

digestion of substrates. In control cells addition of BafA1increased cellular abundance of LC3-II but the exposure of Tay-Sachs fibroblasts to the inhibitor did not affect baseline LC3-II staining, (Figure 1I). These findings strongly suggest that autophagosome processing is defective in these cells.

Autophagosome accumulation with arrested autophagic flux in Tay-Sachs disease

Electron microscopy of fibroblasts obtained from patients with Tay-Sachs disease revealed an extensive accumulation of autophagosomes, an abnormality not present in control cells (Figure 2A and B). The pathological changes, with abundant multilamellar bodies, closely resemble those first reported in neurons obtained from the brains of infants with Tay-Sachs disease [12].

To distinguish between autophagosome–lysosome fusion or inefficient lysosomal degradation as factors in the accumulation of autophagosomes and altered autophagic flux, we examined lysosome–autophagosome fusion using tandem fluorescent-tagged LC3-II as an autophagosomal marker. We observed numerous yellow structures corresponding to autophagosomes in mCherry-GFP-LC3-II-expressing fibroblasts from Tay-Sachs patients, compared with those from control subjects (Figure 2C and E).

Engulfment of mitochondria by lysosomes and their digestion by mitophagy was explored by the use of high-resolution confocal microscopy to co-localise cytochrome C and LC3 (Figura 2D and F). Markedly increased abundance of engulfed, but incompletely digested mitochondria, confirmed that fusion of lysosomes with autophagosomes is impaired - an abnormality that was observed in fibroblasts from patients with Tay-Sachs disease, irrespective of their clinical severity.

Autophagosome accumulation is associated with increased Lysosomal permeability

Degradation of autophagic cargo by acid hydrolases, including cathepsins, occurs in the autophagolysosomal compartment. Impaired autophagic flux with the accumulation of autophagosomes/autophagolysosomes can result from either reduced autophagosome–lysosome fusion or inefficient lysosomal degradation [12]. To distinguish between these mechanisms, we determined whether the impaired autophagic flux in cells affected by Tay-Sachs disease and deficient β-hexosaminidase A activity was associated with decreased activity of other lysosomal acid hydrolases. In this respect, the expression of CatB and CatD was increased in Tay-Sachs fibroblasts. (Figure 3A). To explore the possible role of CatB in the pathophysiology of Tay-Sachs disease, we examined the intracellular localisation of the protein by confocal immunofluorescence microscopy. In healthy fibroblasts, the CatB signal co-localised with the lysosomal membrane marker LAMP-1, indicating that, as expected, it is principally found in the lysosome/autophagolysosome compartment. However, in Tay-Sachs fibroblasts, the CatB immunofluorescence signal occurred diffusely throughout the cytosol and was only partially associated with the LAMP-I marker. These findings suggested that increased lysosome/autophagolysosome membrane permeabilisation is a pathological manifestation of the disease (Figure 3 B and D). Of note, in this context, HexA immunostaining also revealed a diffuse pattern in the cytosol and a similarly reduced co-localisation with the lysosomal membrane marker, LAMP-I (Figure 3C and E). The latter observation was not only unexpected and dependent on the presence of residual immuno-reactivity of some mutant HexA proteins but also may reflect the consequences of protein aggregation.

Increased permeability of lysosomes in mutant fibroblasts was explored further by examining the appearance and distribution of galectin puncta in autophagolysosomes (Supplementary Figure 1). These findings confirmed the enhanced lysosomal

permeability of fibroblasts that we identified in Tay-Sachs disease. Analysis of isolated lysosomes obtained after cell fractionation confirmed the redistribution of HexA antigen with an increased fluorescence signal in the cytosol of Tay-Sachs fibroblasts compared with controls (Figure 3F); this altered distribution was reflected in a relative reduction of the lysosomal component. As depicted in Figure 3 F, redistribution of mutant HexA occurred in fibroblasts in which increased cytosolic abundance of CatB was detected.

Given the organelle pathology that we observed in Tay-Sachs fibroblasts, we examined the subcellular distribution of the master regulator of autophagy and lysosomal biogenesis, Transcription Factor EB (TFEB). In healthy cells, TFEB is normally inactive and diffused in the cytosol in association with the surface of the lysosome, however, when the lysosomal function is inhibited, dephosphorylation of TFEB leads to its translocation to the nucleus where stimulates lysosomal biogenesis by actively upregulating the transcription of target genes harbouring the CLEAR element [13]. As predicted and illustrated in Supplementary Fig 2, immunoreactive TFEB were abundant and concentrated in nuclei of fibroblasts obtained from patients with both subtypes of GM2 gangliosidosis.

Altered mTOR pathway is associated with HexA expression

TFEB is activated under conditions of restricted nutrition and energy generation, and in authentic models of diseases in which lysosomal clearance of intracellular debris is impaired. Given as above that we found subcellular srelocalisation of TFEB from lysosomes to the nucleus in diseased fibroblasts, we investigated the potential engagement of the mechanistic target of rapamycin (mTOR), a kinase and primary regulator of autophagy and lysosomal biogenesis [7,8] in the TFEB translocation process. The down-regulated and phosphorylated forms of p-mTOR and p-AKT were increased in fibroblasts from patients with Tay-Sachs compared with control cells (Figure 4).

Impaired mTOR/autophagy and LMP are also associated with Sandhoff disease

To test the common underlying cellular pathophysiology in GM2 gangliosidosis, we further explored the changes in Sandhoff disease, which is related to Tay-sachs disease but due to mutations in HEXB with consequential effects on the β-subunit shared by the Hex A and Hex B isoenzymes. Fibroblasts obtained from two patients with Sandhoff disease with reduced enzymatic activities and confirmed HEXB mutations were studied (Supplementary Table 1). As with the point mutations detected in the patients with Tay-Sachs disease, those in Sandoff disease were predicted to destabilise the β-hexosaminidase structures (Supplementary Figure 3). Similarly, autophagy was impaired in fibroblasts from these patients with increased LC3-II abundance and, accumulation of p62 and with p-mTOR species (Figure 5A). In addition, we observed increased expression of active CatB and CatD with enhanced release of CatB from the lysosome into the cytosolic compartment (Figure 5A-C) with abundant and concentrated TFEB in nuclei of fibroblasts obtained from patients with Sandhoff (Supplementary Figure 4). Additional confirmation of these pathological effects was provided by the immunofluorescent detection of galectin puncta in autophagolysosomes (Supplementary Figure 5), and identification of abundant multilamellar bodies and appearance of autophagosomes by electron microscopy (Figure 5B and D). To validate our findings *in vivo*, we used a mouse model lacking both Hex A and B activities as a result of targeted disruption of the hex β subunit gene (Sandhoff strain) which is an authentic model of acute human GM2 gangliosidosis (and Tay-Sachs disease). As in the different cellular models, the analysis of brain, spinal cord, brain stem and cerebellum was consistent with marked disruption of autophagy accompanied by inhibition of p-mTOR and increased expression of active cathepsin B, CatB (Figure 5E).

Transcriptomic analysis reveals altered molecular pathways

To better define the molecular pathophysiology of cell injury in Tay-Sachs disease, a microarray expression profiling was carried out on fibroblasts cultured from control subjects and affected patients. Of the 135750 transcripts examined, fibroblasts from patients with the severe infantile variants of the disease showed significant changes in 2141 transcripts when compared with control fibroblasts: 886 transcripts were upregulated and 1255 downregulated. Similar studies in fibroblasts from a patient with the more indolent juvenile variant revealed changes in the abundance of 1327 transcripts: 605 were upregulated, and 722 downregulated. Finally, fibroblasts affected by Sandhoff disease showed changes in the steady-state abundance of 1990 transcripts compared with those from control fibroblasts: 902 transcripts were upregulated, and 1088 downregulated. In-depth pathway analysis indicated changes in the expression of genes encoding proteins engaged in mTOR signalling, autophagy and other lysosomal processes (Table S3-5 and Figure 6 and Supplementary Figure 6 and 7). Significant changes were observed in multiple genes implicated in these pathways. Of note, despite the variability observed between cells from different patients, several changes appear to be related to the pathobiological changes affecting lysosomal function that we report here. Expression of many genes of the mTOR pathway was downregulated, including ATP6V1C1 and Rictor. At the same time, Bcl2, an inhibitor of autophagy [14], and RAB7B, a negative regulator of autophagy flux [15], were upregulated. Arylsulphatase G (ARSG) and aspartylglucosaminidase (AGA), lysosomal enzymes, which are mutated inlysosomal diseases both in animals and humans, were also downregulated. The former changes are compatible with the finding of increased lysosomal permeability [16,17]. Similarly reduced abundance of the LAPTM4B protein has been linked to increased membrane permeability [18].

Of particular relevance, was the increased expression of the phosphoinositide-3-kinase, regulatory subunit 1 (PIK3R1) gene which encodes the regulatory domain (p85α) of the PI3K complex. This change was shared between both subtypes of GM2 gangliosidosis. Accordingly, we returned to the fibroblasts and confirmed the increased abundance of the PI3K protein in the fibroblasts from the patients (Supplementary Figure 8). PI3K induces the phosphorylation of AKT and mTOR, but the phosphorylated forms of both were decreased; we propose that the enhanced expression of PI3K transcripts may reflect a compensatory change related to downregulation of the PI3K/AKT/mTOR pathway. To explore this phenomenon further, we investigated the kinase, PTEN, which canonically regulates the PI3K signalling cascade in a negative manner, thereby dampening downstream AKT/mTOR signalling [19]. According to our hypothesis, PTEN gene transcripts were overexpressed in fibroblasts from patients with GM2 gangliosidosis, compared with cells from control subjects (Supplementary Figure 8).

Arginine treatment recovers mTOR activity and lysosomal dysfunction

As a component of the master-regulator, mTOR complex 1 (mTORC1), mTOR links the availability of nutrients with cell growth and autophagy. Since mTORC1 activity is modulated by growth factors, stress, energy status and amino acids [20], and its function is altered in fibroblasts obtained from patients with Tay-Sachs and Sandhoff Diseases, we sought to determine whether it represents a potential therapeutic target.

Accordingly, we explored the effects of modulating mTOR activity by supplementing fibroblast cultures with amino acids. First, we evaluated the effect of the natural amino acids, L-arginine and L-leucine as well as acetyl-DL-leucine, a modified, cell-penetrant amino acid which has been shown to improve clinical symptoms in Niemann-Pick type C patients [21]. Under the experimental conditions used, L-arginine treatment significantly increased the rate of cell growth in fibroblasts obtained from patients with both GM2

gangliosidosis sub-types (Supplementary figure 9). It was notable that this improvement was not observed with either L-leucine (Supplementary figure 10) or acetyl-DL-leucine (Supplementary figure 11).

To understand the apparent specificity of the arginine effect *in vitro*, we conducted a more intensive analysis of the transcriptomic findings in GM2 gangliosidosis fibroblasts: this revealed changes in the expression of several genes that encode enzymes involved in arginine biosynthesis (Supplementary figure 12A-C and Table S6). On account of this finding, we searched for indicators of altered arginine metabolism in patients with Tay-Sachs and Sandhoff disease. Concentrations in serum of L-arginine and nitric oxide (generated from arginine by the action of nitric oxide synthases) were moderately reduced in patients (Supplementary figure 15A-C). The most significant change in the transcriptomic analysis of arginine biosynthesis was argininosuccinate synthetase (ASS1), the third enzyme of the urea cycle which catalyses the formation of argininosuccinate from aspartate, citrulline, and ATP. Located on the outer mitochondrial membrane, ASS1 is the rate-limiting step for the formation of arginine *de novo* and a source of this substrate for nitric oxide synthases [22]. The transcriptomic findings in Tay-Sachs and Sandhoff were confirmed by reduced expression of ASS1 protein (Supplementary figure 12D-F). These findings raise the possibility that alterations in arginine biosynthesis contribute to the pathophysiology of these diseases.

On the other hand, the mTOR pathway was partially rescued in patients with Tay-Sachs disease after 120 hours of exposure to L-arginine with a boost in the reduced protein synthesis of the patients (Figure 7A and B). These observations were also mirrored in fibroblasts from patients with Sandhoff disease (Supplementary Figure 13A). Furthermore, we examined lysosome–autophagosome fusion. A significantly reduced number of yellow structures that correspond to autophagosomes was evident in mCherry-

GFP-LC3-expressing Tay-Sachs fibroblasts after L-arginine treatment (Figure 7C). These results confirmed that mTOR activity and the fusion of autophagosomes and lysosomes could be improved by supplementation with L-arginine.

Given that altered lysosomal membrane permeability may be a critical factor in the pathophysiological alterations found in cells from patients with GM2 disease, we next evaluated the effects of L-arginine treatment on CatB release from lysosomes. Treatment with L-arginine induced a marked reduction in CatB expression levels in Tay-Sachs fibroblasts (Figure 8A), as well as an increased co-localisation of CatB signal with the LAMP-1 marker, suggesting the restitution of the permeability barrier (Figure 8A and C). A significant increase in HexA co-localisation with LAMP-1 was observed alongside the elevated expression of the mature form of HexA (Figure 8B and C) - findings shared between Tay-Sachs and Sandhoff diseases. (Supplementary Figure 13B). To test whether the supplementation with L-arginine suppressed autophagy, by complementing the supply of amino acids, we examined the effects on TFEB localization. After the addition of L-arginine, there was a notable decrease in the presence of nuclear TFEB an effect which would lead to a reduced transcriptional drive towards lysosomal biogenesis (Supplementary Figure 14).

Finally, as an early exploration of proof of concept, two patients suffering from juvenile forms of Tay-Sachs and Sandhoff diseases TSD2 and Juvenile SD2) consented to take oral supplements of L-arginine (0.3g/Kg/day) for 8 months. Although it was not possible to provide an objective evaluation of the neurological outcomes, family carers and physiotherapists reported improved coordination in both patients and suggested that their rate of cognitive deterioration was partially arrested. The effects of L-arginine supplementation were explored in mononuclear blood cells obtained from these patients. As shown in Figure 8D, administration of oral L-arginine partially restored mTOR

expression. Moreover, the pathological abundance of cathepsin B was suppressed and accompanying this, the expression of HexA and arginosuccinate lyase protein in these cells was improved.

Discussion

Despite many initiatives, no treatment of proven safety and efficacy is available for patients stricken by any clinical subtype of GM2 gangliosidosis. While the genetic and biochemical basis for this disease have been well studied, an integrated description of its pathogenesis and the sequence of unitary steps that lead to its destructive neuroinflammatory effects is lacking. To explore the pathophysiological complexity of these sphingolipid diseases, we used living cells as a focus for a comprehensive molecular characterisation of their disordered cell biology. This platform facilitated corroborative investigations in the coherent model of these disorders in the genetically modified mouse, followed by early proof-of-concept studies carried out in two affected patients.

Here we describe metabolic derangements that accompany markedly impaired autophagy in human fibroblasts harbouring pathological defined HEXA and HEXB mutations. The diseased cells had poor growth rates in culture. Thus, they showedreduced ATP concentration and energy charge together with disrupted mitochondrial electron-transport and suffered oxidative stress. Despite the florid appearance of autophagic vacuoles, the accompanying increase of LC3-II protein might indicate either an enhanced autophagic drive or, as here, also with enhanced p62/SQSTM1 expression, impaired autophagic flux [23]. Blocked autophagic flux was confirmed by a BafA1 assay and by ultrastructural appearances. We noted, that defective autophagic degradation or interruption in autophagic flux has been shown in several lysosomal diseases such as Niemann-Pick disease type C, Gaucher and Pompe diseases [24-27].

Numerous abnormalities have been reported in association with lysosomal dysfunction. These include: changes in lysosomal enzymes, the volume and number of lysosomes and in membrane properties. All these abnormalities represent or drive the loss of functionalityincluding autophagy [28]. For example a reduction in members of the family of cysteine proteinases such as CatC and CatL, have been related to a compensatory transcriptional upregulation of CatB expression due to TFEB as well as autophagy dysfunction [29,30]. Furthermore, in Niemann-Pick disease C, the increased expression of mature protein forms for both CatB and CatD are associated with the build-up of autophagosomes [31].

Here we found that the deficiency of HexA was associated with a compensatory upregulation of mature CatB, CatD and lysosomal permeabilisation. Furthermore, this permeabilisation was associated with the release of CatB and HexA. The pent-up machinery of autophagy and effects on intracellular metabolism are likely to have a strong bearing on the pathophysiology of this disease, given that florid end-stage changes are prominent neuropathological features that presage cell death in affected neurons distributed throughout the nervous system in the last phases of illness in patients with Tay-Sachs and Sandhoff diseases [28,31,32]. , In its terminal phase, deranged autophagy is likely to contribute additionally to the pathological cascade by stimulating release of inflammatory cytokines through the agency of the p62/SQSTM1 signal [9]. As to the upstream drive to enhance autophagosome genesis in Tay-Sachs and Sandhoff diseases, we find evidence that this is due to nuclear translocation of TFEB, since it activates genes that orchestrate lysosomal biogenesis. The critical discovery of this fundamental process emerged from the brilliant realization that coordinated lysosomal expression and regulation (CLEAR) represented a gene network which could be controlled by a single major transcriptional factor that recognized a key regulatory element common to effector

proteins fundamentally implicated in lysosomal pathobiology [33]. The complex disturbance of lysosomal structure and function in fibroblasts from Tay-Sachs and Sandhoff patients as a consequence of reduced activity of the lysosomal β-hexosaminidases with increased autophagosome size can be attributed to TFEB activation as part of a response that will drive compensatory expansion of the lysosomal compartment. The enhanced TFEB nuclear localization, we reported here in Tay-Sachs and Sandhoff fibroblasts is fully compatible with this process [33]. In this context we further explored the potential engagement of the multifunctional mTOR pathway as and found reduced basal activity of mTOR: the changes in cultured fibroblasts were recapitulated and widely distributed in central nervous system of the genetically coherent model of GM2 gangliosidoses in the Sandhoff strain mouse. Analysis of brain, spinal cord, brain stem and cerebellum revealed the same pathobiological abnormalities: diminished mTOR activity associated with reduced protein synthesis and increased autophagy. In this context it is notable that compensatory changes in mTOR activity have been reported in other Lysosomal storage disorders, including mucopolysaccharidosis type 2, Fabry disease, aspartylglucosaminuria and Pompe diseases in which impaired mTOR reactivation is associated with defective lysosome reformation [7,34]. Reduced basal mTOR activity has also been observed in diverse models of lysosomal diseases including Neuronal Ceroid Lipofuscinosis type 3 lymphoblastoid cells [35], in NPC1- and NPC2-knockdown endothelial cells [36], in a Drosophila model of mucolipidosis IV [37], and a human podocyte model of Fabry disease [38].

Autophagy is a constitutive but dynamically controlled process that is central to the maintenance of cellular homeostasis. Any disturbance of lysosomal function, as in the genetic disorders, Tay-Sachs and Sandhoff diseases will require compensatory adjustments to ensure, so far as possible, survival of the affected cell. These GM2

gangliosidoses, which preferentially affect the lyososomal recycling of membrane-derived sphingolipids abundant in neurons, provide a spectacular example of the rôle of autophagy in non-mitotic cells with a life-long dependence on mitochondrial energy generation: relentlessly progressive, these diseases cause widespread neuronal death. [39]. Our findings provide evidence for a mechanistic link between disrupted autophagy, increased permeabiization of the lysosomal compartment and neuro-inflammatory changes [40,41].

We contend that the pathological mTOR signalling and consequential mitochondrial and lysosomal dysfunction that we report in GM2 gangliosidosis immediately suggest avenues for therapeutic exploration. Amino acid supplementation to restore mTOR activity has been investigated in Pompe disease: arginine and leucine were found to restore mTOR signalling and partiallyrescuedthe muscle disease due to gross failure of glycogen remodeling and with the accumulation of pathological autophagosomes in the sarcoplasm [7]. In our studies with fibroblasts obtained from affected patients, improvement of the cell phenotype was found to be specific for L-arginine, rather than L-leucine, and we attribute this specificity to the consistent genetic changes in a rate-limiting enzyme of L-arginine biosynthesis (arginosuccinate lyase) prompted by gene expression studies carried out in fibroblastsfrom patients with Tay-Sachs and Sandhoff diseases. Given that the patients have neurological dysphagia and in many cases feeding-tube placement, we at first considered that the reduced serum arginine concentrations might reflect a nutritional defect, especially in the most severely affected infants. However, our studies of fibroblasts were conducted in cells obtained after prolonged outgrowth culture of skin biopsy samples. In these, microarray analysis revealed a specific alteration related directly to a rate-limiting enzyme in arginine biosynthesis. The previousfindings were

corroborated by the reduced abundance of human argino-succinate synthetase protein in fibroblast extracts.

Tay-Sachs and Sandhoff diseases are paradigmatic examples of a large class of lysosomal diseases that are scharacterised by unremitting neurodegeneration. Unfortunately, treatments can only address symptoms and management is directed towards supporting critical functions that are progressively lost. For these reasons, the conditions remain a focus of research-based principally on molecular therapies [9]. Our study considers a molecular approach that has not been explored in these diseases but is based on a fresh examination of the pathobiology of the disease. If adopted in practice, the approach is non-invasive and could be readily adapted to practical clinical care that includes a focus on nutrition. While it is an essential amino acid and natural dietary constituent, L-arginine has potent biological effects, for example on the formation of nitric oxide (for which it is the primary substrate) and in non-physiological doses has potential toxicity exerted by this and other mechanisms. Thus, any clinical use of L-arginine supplements would necessitate careful consideration, including approval from appropriate regulatory authorites and with the benefit of informed professional advice. However, modulation of mTOR with a physiological compound, L-arginine, if effective offers a largely non-invasive option for opportune exploration in GM2 gangliosidosis. After further clinical research, since it appears to have salutary effects on the cellular environment and attenuates the pathological release of cathepsins and other components of the lysosomal armoury, L-arginine might also be considered as an adjunct to definitive molecular therapies that directly address the genetic defect and are in development [8,9]. Here we conclude that our *in vitro* and *in vivo* studies call for further scientific exploration to support early-stage clinical studies. Furthermore, we corroborate the *in vitro* data after l-

arginine treatment, and we can think about the possibility to design new therapeutic studies with arginine.

Acknowledgments

This study was supported by a grant from the Spanish Association of families affected by Tay-Sachs and Sandhoff disease (ACTAYS). BC was the recipient of a studentship from the Spanish Association of families affected by Tay-Sachs and Sandhoff disease (ACTAYS). BC was also supported by a studentship from TRANSAUTOPHAGY network.

Conflict of interests

All the authors declare that no conflict of interest exists for any of them.

References

1. De Duve, C., Wattiaux, R. (1966). Functions of lysosomes. Annu Rev Physiol. 28,435-92.
2. Nakatogawa, H., Suzuki, K., Kamada, Y., Ohsumi, Y. (2009). Dynamics and diversity in autophagy mechanisms: lessons from yeast. Nat Rev Mol Cell Biol. 10,458-67.
3. Jiang, P., Mizushima, N. (2014). Autophagy and human diseases. Cell Res. 24,69-79.
4. Ballabio, A., Bonifacino, J.S. (2019). Lysosomes as dynamic regulators of cell and organismal homeostasis. Nat Rev Mol Cell Biol. 21,101-118.
5. Munson, M.J., Ganley, I.G. (2015). MTOR, PIK3C3, and autophagy: Signaling the beginning from the end. Autophagy. 11,2375-6.
6. Settembre, C., Zoncu, R., Medina, D.L., et al. (2012). A lysosome-to-nucleus signalling mechanism senses and regulates the lysosome via mTOR and TFEB. EMBO J. 31,1095-108.
7. Lim, J.A., Li, L., Shirihai, O.S., et al. (2017). Modulation of mTOR signaling as a strategy for the treatment of Pompe disease. EMBO Mol Med. 2017;9:353-370.
8. Cachon-Gonzalez., M.B., Zaccariotto, E., Cox, T.M. (2018). Genetics and Therapies for GM2 Gangliosidosis. Curr Gene Ther. 18,68-89.
9. Solovyeva, V.V., Shaimardanova, A.A., Chulpanova, D.S, et al. (2018). New Approaches to Tay-Sachs Disease Therapy. Front Physiol. 9,1663.
10. Wildeman, M., van Ophuizen, E., den Dunnen, J.T., Taschner, P.E. (2008). Improving sequence variant descriptions in mutation databases and literature using the Mutalyzer sequence variation nomenclature checker. Hum Mutat. 29, 6-13.

11. Tropak, M.B., Reid, S.P., Guiral, M., Withers, S.G., and Mahuran, D. (2004). Pharmacological enhancement of b-hexosaminidase activity in fibroblasts from adult Tay-Sachs and Sandhoff Patients. J. Biol. Chem. 279,13478–13487.
12. Terry, R.D., Korey, S.R. (1960). Membraneous cytoplasmic granules in infantile amaurotic idiocy. Nature. 188, 1000-1002.
13. Napolitano, G., Ballabio, A. (2016). TFEB at a glance. J Cell Sci. 129,2475-81.
14. Marquez, R.T., Xu, L. (2012). Bcl-2:Beclin 1 complex: multiple, mechanisms regulating autophagy/apoptosis toggle switch. Am J Cancer Res. 2,214-21.
15. Kjos, I., Borg Distefano, M., et al. (2017). Rab7b modulates autophagic flux by interacting with Atg4B. EMBO Rep. 18,1727-1739.
16. Kowalewski, B., Heimann, P., Ortkras, T., et al. (2015). Ataxia is the major neuropathological finding in arylsulfatase G-deficient mice: similarities and dissimilarities to Sanfilippo disease (mucopolysaccharidosis type III). Hum Mol Genet. 24,1856-68.
17. Arvio, M., Mononen, I. (2016). Aspartylglycosaminuria: a review. Orphanet J Rare Dis. 11,162.
18. Li, Y., Zhang, Q., Tian, R., et al. (2011). Lysosomal transmembrane protein LAPTM4B promotes autophagy and tolerance to metabolic stress in cancer cells. Cancer Res. 71,7481-9.
19. Yehia, L., Ngeow, J., Eng, C. (2019). PTEN-opathies: from biological insights to evidence-based precision medicine. J Clin Invest. 129,452-464.
20. Jewell, J.L., Russell, R.C., Guan, K.L. (2013). Amino acid signalling upstream of mTOR. Nat Rev Mol Cell Biol. 14,133-9.
21. Bremova, T., Malinová, V., Amraoui, Y., et al. (2015). Acetyl-dl-leucine in Niemann-Pick type C: A case series. Neurology. 85,1368-75.

22. Diez-Fernandez, C., Rüfenacht, V., Häberle, J. (2017). Mutations in the Human Argininosuccinate Synthetase (ASS1) Gene, Impact on Patients, Common Changes, and Structural Considerations. Hum Mutat. 38,471-484.
23. Klionsky, D.J., Abdelmohsen, K., Abe, A., et al. (2016). Guidelines for the use and interpretation of assays for monitoring autophagy (3rd edition), Autophagy. 12,1–222.
24. Guo, H., Zhao, M., Qiu, X., et al. (2016). Niemann-Pick type C2 deficiency impairs autophagy-lysosomal activity, mitochondrial function, and TLR signaling in adipocytes. J Lipid Res. 57,1644-58.
25. Sarkar, S., Carroll, B., Buganim, Y., et al. (2013). Impaired autophagy in the lipid-storage disorder Niemann-Pick type C1 disease. Cell Rep. 5, 1302-15.
26. Aflaki, E., Moaven, N., Borger, D.K., et al. (2016). Lysosomal storage and impaired autophagy lead to inflammasome activation in Gaucher macrophages. Aging Cell. 15,77-88.
27. Spampanato, C., Feeney, E., Li, L., et al. (2013). Transcription factor EB (TFEB) is a new therapeutic target for Pompe disease. EMBO Mol Med. 5,691-706.
28. Wang, F., Gómez-Sintes, R., Boya, P. (2018). Lysosomal membrane permeabilization and cell death. Traffic. 19,918-931.
29. Bullón, P., Castejón-Vega, B., Román-Malo, L., et al. (2018). Autophagic dysfunction in patients with Papillon-Lefèvre syndrome is restored by recombinant cathepsin C treatment. J Allergy Clin Immunol. 142,1131-1143.e7.
30. Mizunoe, Y., Sudo, Y., Okita, N., et al. (2017). Involvement of lysosomal dysfunction in autophagosome accumulation and early pathologies in adipose tissue of obese mice. Autophagy. 13,642-653.

31. Liao, G., Yao, Y., Liu, J., et al. (2007). Cholesterol accumulation is associated with lysosomal dysfunction and autophagic stress in Npc1 −/− mouse brain. Am J Pathol. 171,962-75.

32. Wang, F., Gómez-Sintes, R., Boya, P. (2018). Lysosomal membrane permeabilization and cell death. Traffic. 19, 918-931.

33. Sardiello, M., Palmieri, M., di Ronza, A., et al. (2009). A gene network regulating lysosomal biogenesis and function. Science. 325,473-7.

34. Yu, L., McPhee, C.K., Zheng, L., et al. (2010). Termination of autophagy and reformation of lysosomes regulated by mTOR. Nature. 465,942-6.

35. Cao, Y., Espinola, J.A., Fossale, E., et al. (2006). Autophagy is disrupted in a knock-in mouse model of juvenile neuronal ceroid lipofuscinosis. J Biol Chem. 281,20483 – 20493.

36. Xu, J., Dang, Y., Ren, Y.R., Liu, J.O. (2010). Cholesterol trafficking is required for mTOR activation in endothelial cells. Proc Natl Acad Sci USA. 107, 4764 – 4769.

37. Wong, C.O., Li, R., Montell, C., Venkatachalam, K. (2912). Drosophila TRPML is required for TORC1 activation. Curr Biol. 22,1616 – 1621.

38. Liebau, M.C., Braun, F., Hopker, K., et al. (2013). Dysregulated autophagy contributes to podocyte damage in Fabry's disease. PLoS ONE. 8, e63506.

39. Merscher, S., Fornoni, A. (2014). Podocyte pathology and nephropathy - sphingolipids in glomerular diseases. Front Endocrinol (Lausanne). 5,127.

40. Utz, J.R., Crutcher, T., Schneider, J., et al. (2015). Biomarkers of central nervous system inflammation in infantile and juvenile gangliosidoses. Mol Genet Metab. 114,274-80.

41. Pišlar, A., Kos, J. (2014). Cysteine cathepsins in neurological disorders. Mol Neurobiol. 49,1017-30.

Figures

Figure 1. Model structures of HexA (PDB:2GJX) and HexB (PDB:1NOU) sub-unit proteins, highlighting the location of pathogenic mutations. Also shown autophagy in fibroblasts obtained in culture from patients with GM2 gangliosidosis (Tay-Sachs and Sandhoff diseases). **A.** HexA point mutations: different colours depict amino acid substitutions identified in the cognate structures identified in different mutations studied. **B.** Frameshift mutations in the alpha subunits found in two patients with Tay-Sachs disease are shown in yellow and orange; premature stop codons are marked by an asterisk. **C.** The surface of hexosaminidase A with the critical active site region required for hydrolysis of GM2 ganglioside (CRH_GM2). The propeptide is shown in grey and the mature protein chain is depicted in white. **D.** Enzymatic activity of HexA in fibroblast homogenates. **E.** Morphological changes in fibroblasts from Tay-Sachs patients compared with control cells. **F.** Cell growth determined in healthy and Tay-Sachs fibroblasts. **G.** Expression of autophagy proteins in control and Tay-Sachs fibroblasts: LC3-I (top panels, top band), LC3-II (top panels, bottom band). **H.** Immunofluorescence staining with anti-p62 antibody. **I.** Impaired autophagic flux in Tay-Sachs fibroblasts. Determination of LC3-II in the presence and absence of bafilomycin A1 in control (CTL) and fibroblasts from Tay-Sachs patients; bafilomycin A1 was used at a final concentration of 100 nM with 12 h exposure. Total cellular extracts were analysed by immunoblotting with antibodies against LC3. The data are the mean ± SD for experiments conducted on two different control cell lines. Data represent the mean ± SD of three separate experiments. ***$p < 0.001$, **$p < 0.005$, *$p < 0.05$ between cells from control subjects and patients with Tay-Sachs disease.

Figure 2. A. Control fibroblasts and those from patients with Tay-Sachs disease showing typical ultrastructure with several distinct lamellar bodies (black arrows); white arrows indicate autophagosomes. Scale bar 10 µm (low magnification) and 2 µm (high magnification). **B.** Quantitative analysis of autophagosomes. **C and E.** Representative image of fibroblasts after transfection of the dual-labelled mCherry-GFP-LC3 plasmid and quantification of autophagic puncta (see Methods). **D and F.** Immunofluorescence of LC3 and cytochrome c in control and pathological cells and quantification of mitophagy puncta. Data represent the mean – SD of three separate experiments. ***p < 0.001, **p < 0.005, *p < 0.05 between controls and Tay-Sachs patients

Figure 3. A. Expression of CatB, CatD and HexA protein were determined in control fibroblasts and those cultured from patients with Tay-Sachs disease. **B and D.** Immunofluorescence of CatB in control and pathological cells and quantification. **C and E.** Immunofluorescence of HexA in control and Tay-Sachs cells with signal quantification. Note that in Tay-Sachs fibroblasts CatB and HexA immunoreactivity is diffused throughout the cytosol. **F.** Cellular fractionation with the isolation of cytosol and lysosomes and protein expression of CatB B and HexA. For control cells, results from two different control cell lines. Data represent the mean±SD of three separate experiments.*P < 0.05; **P < 0.01; **P < 0.001 between control and patients with Tay-Sachs disease.

Figure 4. Expression of mTOR and AKT protein were determined in cultured control and Tay-Sachs disease fibroblasts. Data represent the mean±SD of three separate experiments.*P < 0.05; **P < 0.01; **P < 0.001 between transfected and non-transfected cells.

Figure 5. A. Expression of LC3, p62, CatB, CatD, mTOR and AKT proteins determined in human control and Sandhoff disease fibroblasts. **B and C.** Immunofluorescence of CatB in control and pathological cells with quantification in Sandhoff disease fibroblasts. **B and D.** Characteristic ultrastructure with altered autophagosome abundance quantified in Sandhoff disease fibroblasts. **E.** Expression of LC3, p62, CatB and mTOR proteins in the brain and spinal cord obtained from wild type and hexb $^{-/-}$ mutant mice with GM2 gangliosidosis (Sandhoff disease). Densitometry results are presented as means ± SEM, n = 10 mice. *P < 0.05; **P < 0.01; **P < 0.001 between control and diseased fibroblasts and wild type and hexB $^{-/-}$ mutant mice.

Figure 6. Heatmap clustering of enrichment (z-scores) of the mTOR functions **(A)** and autophagy **(B)** in set of coding genes differentially expressed between control and diseased fibroblasts (n = 3 per case).

Figure 7. A. Expression of mTOR and AKT determined in control and representative Tay-Sachs fibroblasts after L-arginine treatment. **B.** Protein synthesis was quantified in extracts of control and Tay-Sachs fibroblasts treated with L-arginine using puromycin labeling followed by immunoblotting. **C.** Representative image of Tay-Sachs treated fibroblasts after transfection of the mCherry-GFP-LC3 plasmid and quantification of autophagic puncta. For control cells, the data are the mean ± SD for experiments conducted on two different control cell lines. GAPDH was used as a loading control. Data represent the mean±SD of three separate experiments. *P < 0.05; **P < 0.01; **P < 0.001 between control and Tay-Sachs fibroblasts; ^{a} P < 0.05; ^{aa} P < 0.01; ^{aaa} P < 0.001 between non-treated and treated cells.

Figure 8. A and B. Immunofluorescence of CatB and HexA in control and Sandhoff disease fibroblasts and quantification after L-arginine treatment. **C.** Expression of CatB

and HexA protein were determined in control and representative Tay-Sachs fibroblast cultures after L-arginine treatment *in vivo*. **D.** Expression of mTOR, CatB and ASS1 (arginosuccinate synthetase) proteins was determined in peripheral blood mononuclear cells obtained from a patient with juvenile Tay-Sachs disease and a patient with juvenile Sandoff disease after oral L-arginine treatment. Data represent the mean±SD of three separate experiments.*$P < 0.05$; **$P < 0.01$; **$P < 0.001$ between control and Tay-Sachs patients; $^{a}P < 0.05$; $^{aa}P < 0.01$; $^{aaa}P < 0.001$ between non-treated and treated cells.

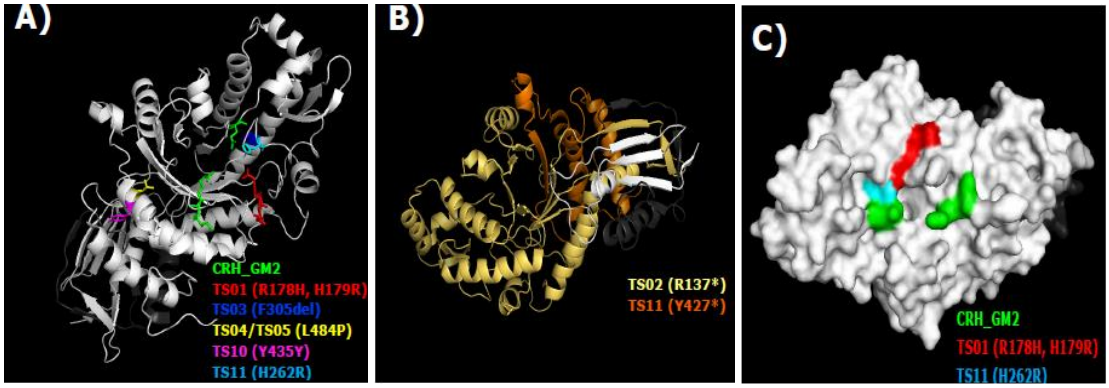

D

Patients	nmol/h/mg prot
CTL	61-316
Inf 1	4
Inf 2	1
Inf 3	7,2
Juv 1	3
Juv 2	9,1
Juv 3	3,8

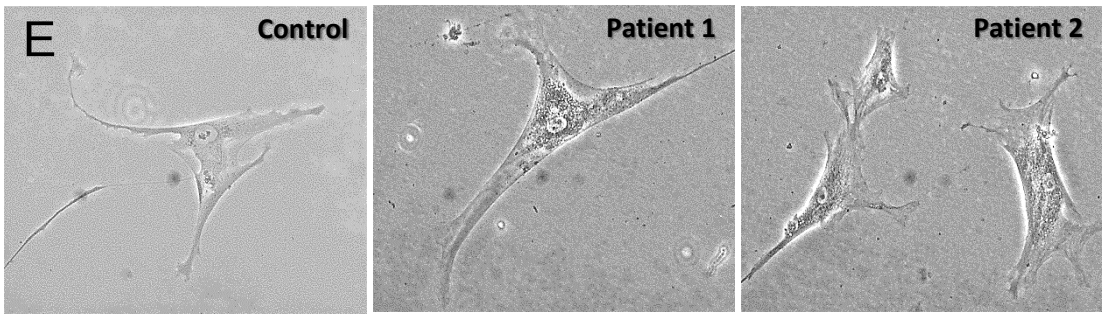

F

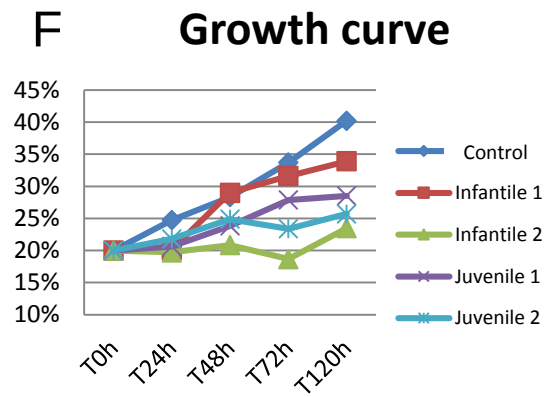

G

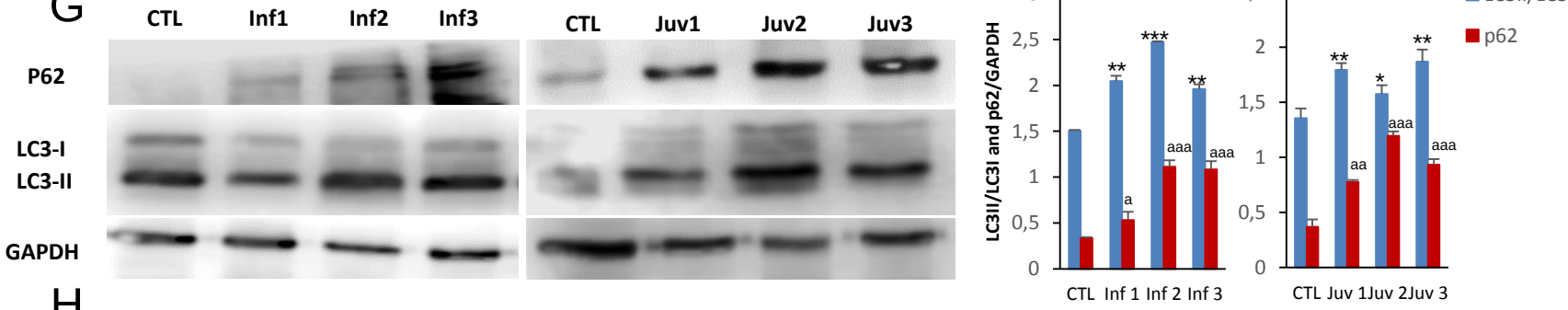

H

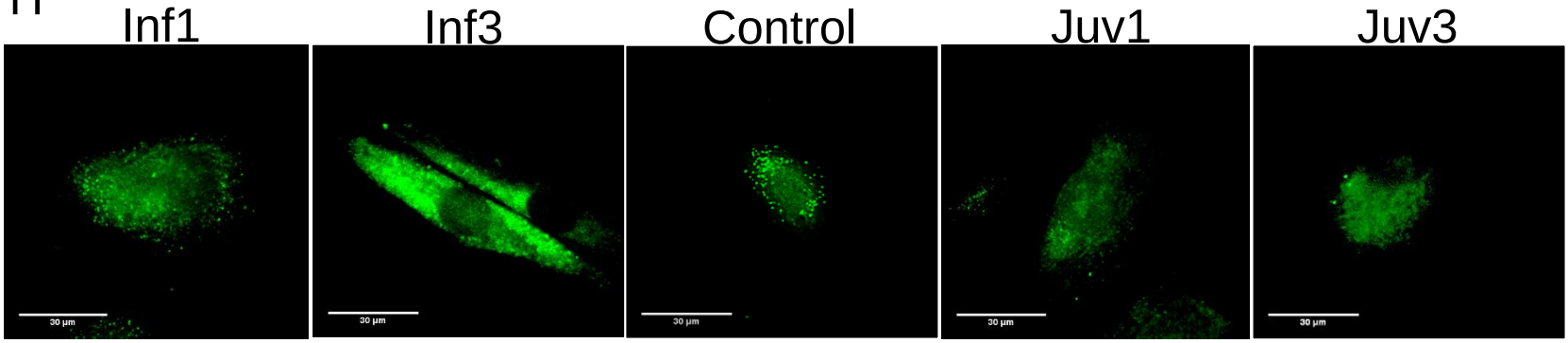

I

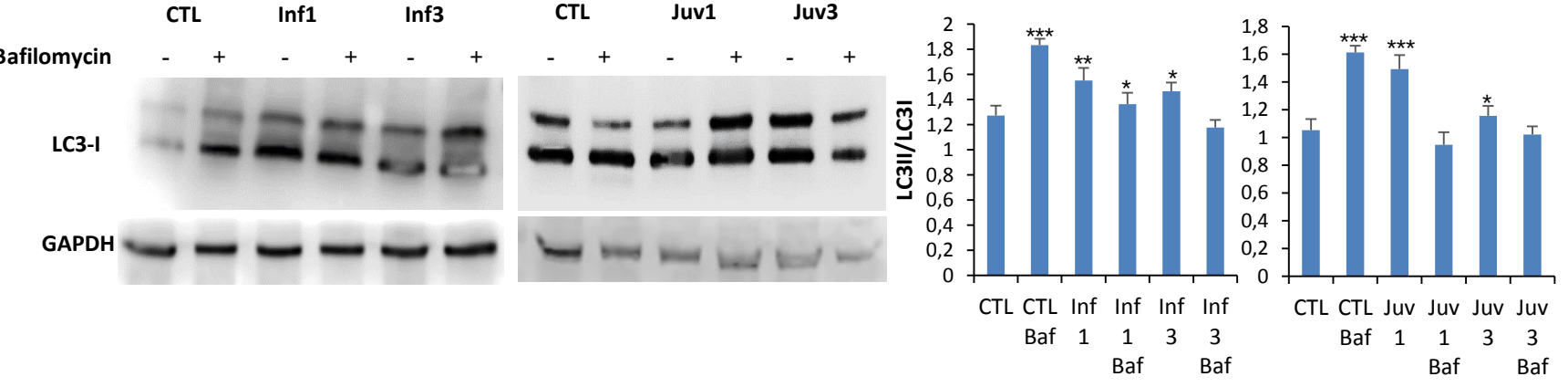

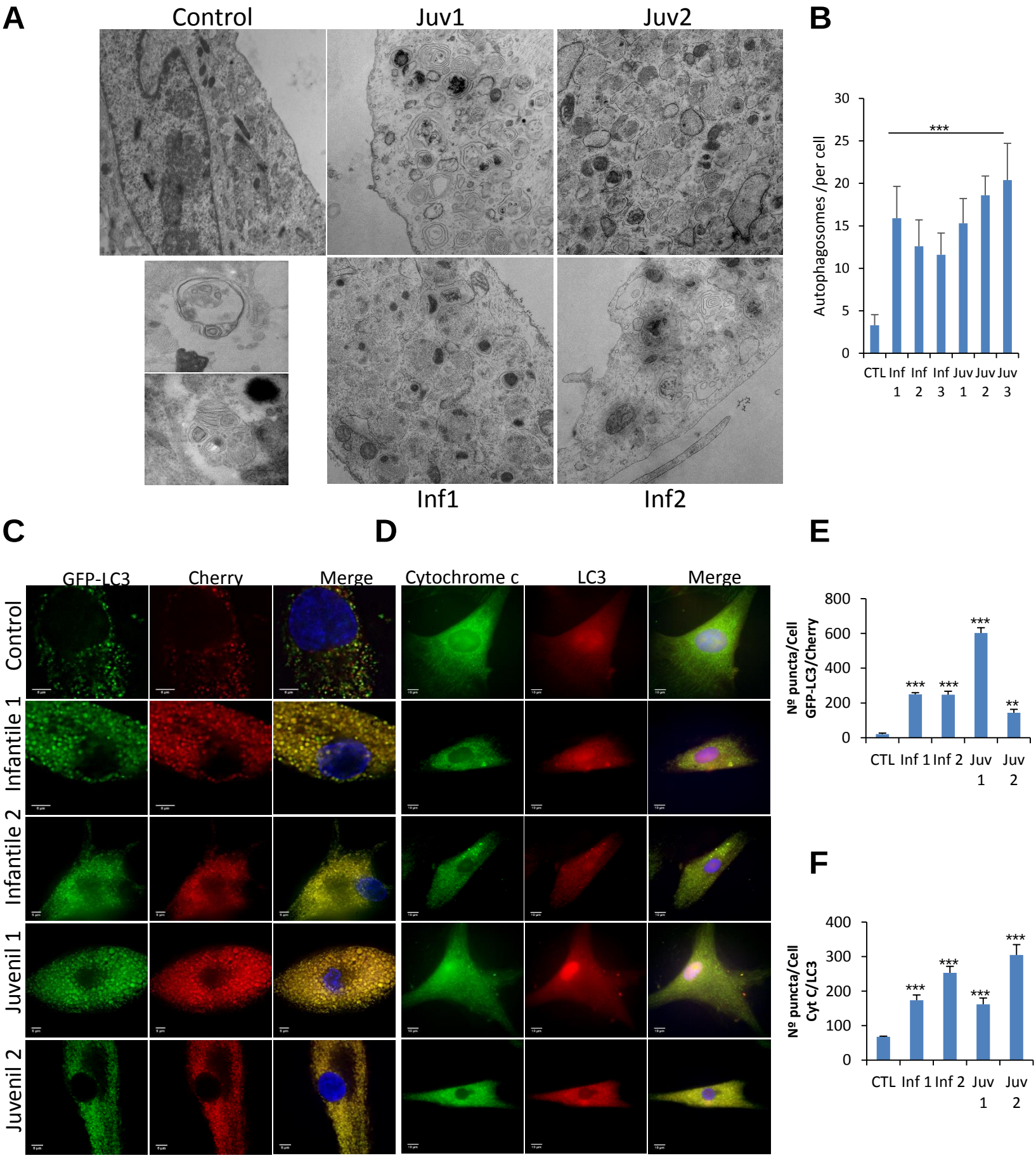
A
Control
Juv1
Juv2
Inf1
Inf2
B
Autophagosomes /per cell
30
25
20
15
10
5
0
***
CTL
Inf 1
Inf 2
Inf 3
Juv 1
Juv 2
Juv 3
C
GFP-LC3
Cherry
Merge
Control
Infantile 1
Infantile 2
Juvenil 1
Juvenil 2
D
Cytochrome c
LC3
Merge
E
Nº puncta/Cell GFP-LC3/Cherry
800
600
400
200
0
***
**
CTL
Inf 1
Inf 2
Juv 1
Juv 2
F
Nº puncta/Cell Cyt C/LC3
400
300
200
100
0
***
CTL
Inf 1
Inf 2
Juv 1
Juv 2

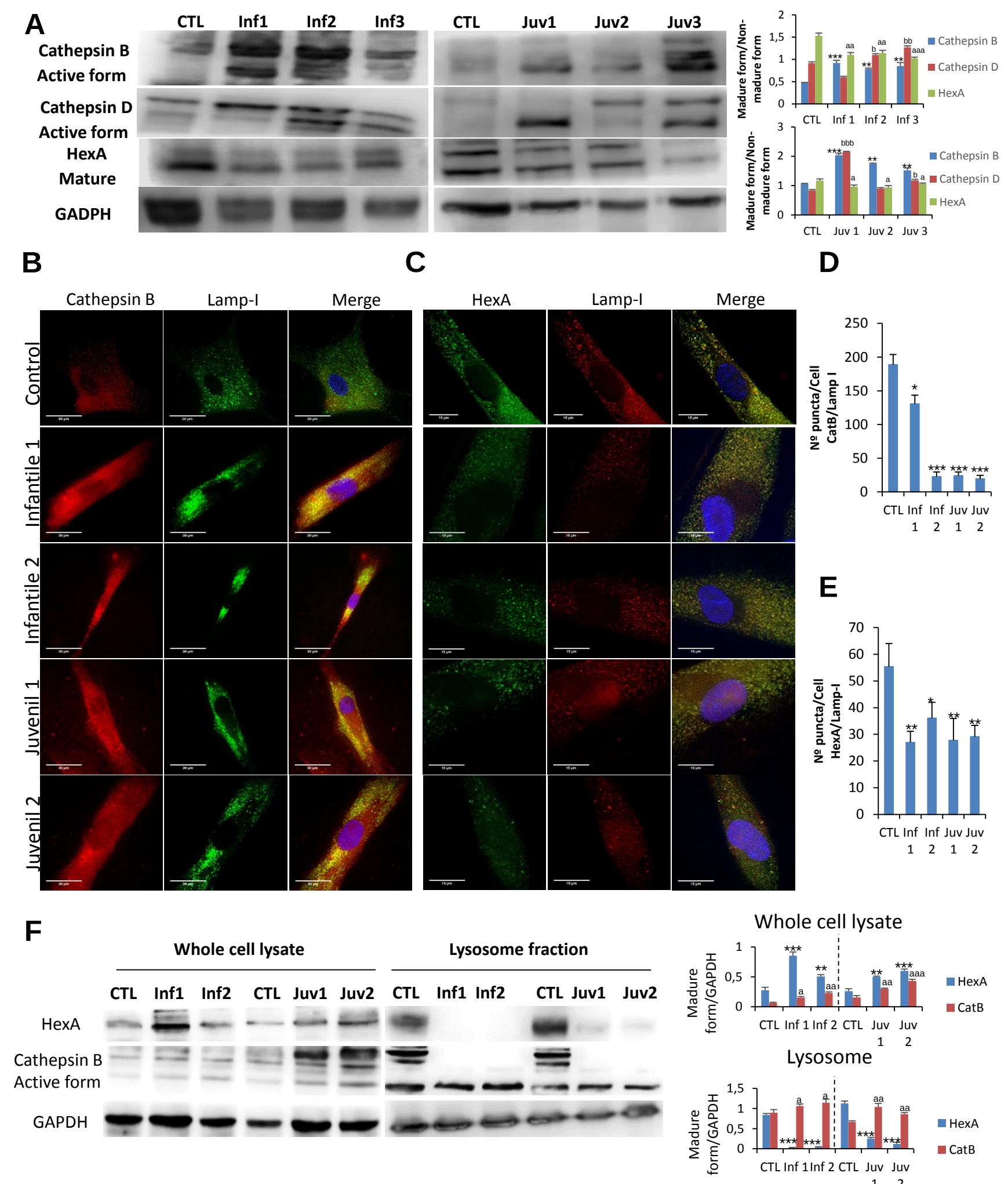
A
CTL
Inf1
Inf2
Inf3
CTL
Juv1
Juv2
Juv3
Cathepsin B
Active form
Cathepsin D
Active form
HexA
Mature
GADPH
Madure form/Non-madure form
Cathepsin B
Cathepsin D
HexA
CTL
Inf 1
Inf 2
Inf 3
Juv 1
Juv 2
Juv 3
B
C
D
Cathepsin B
Lamp-I
Merge
HexA
Lamp-I
Merge
Control
Infantile 1
Infantile 2
Juvenil 1
Juvenil 2
Nº puncta/Cell CatB/Lamp I
Nº puncta/Cell HexA/Lamp-I
E
F
Whole cell lysate
Lysosome fraction
HexA
Cathepsin B
Active form
GAPDH
Madure form/GAPDH
Whole cell lysate
Lysosome
HexA
CatB

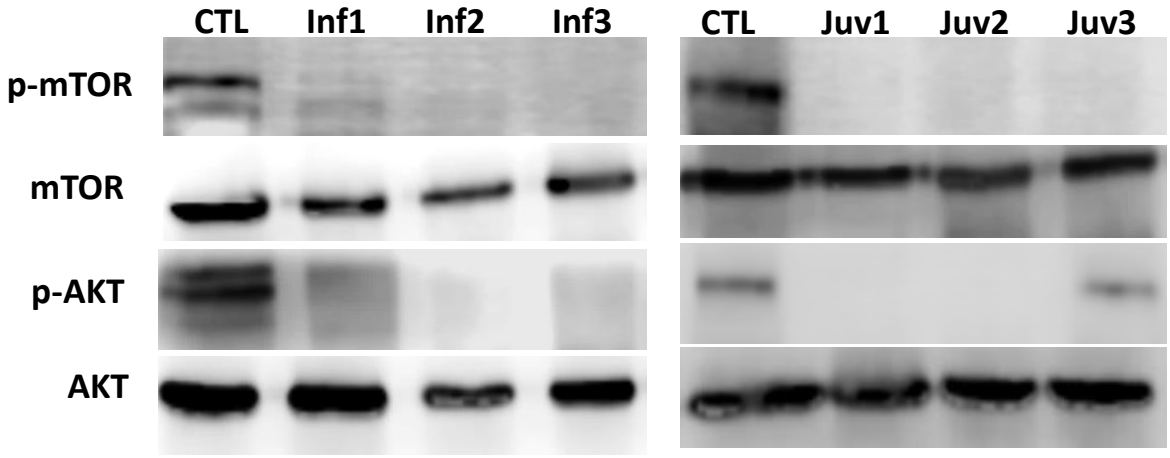
CTL
Inf1
Inf2
Inf3
CTL
Juv1
Juv2
Juv3
p-mTOR
mTOR
p-AKT
AKT

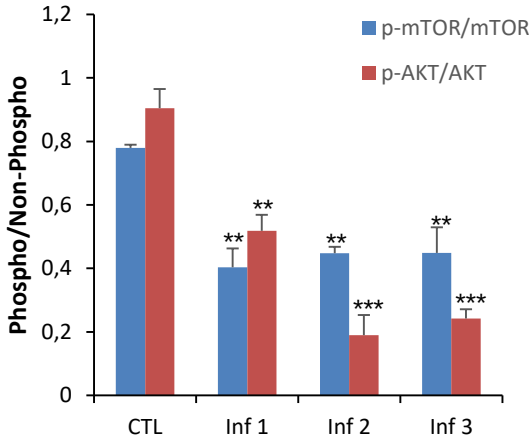
p-mTOR/mTOR
p-AKT/AKT
Phospho/Non-Phospho
1,2
1
0,8
0,6
0,4
0,2
0
CTL
Inf 1
Inf 2
Inf 3

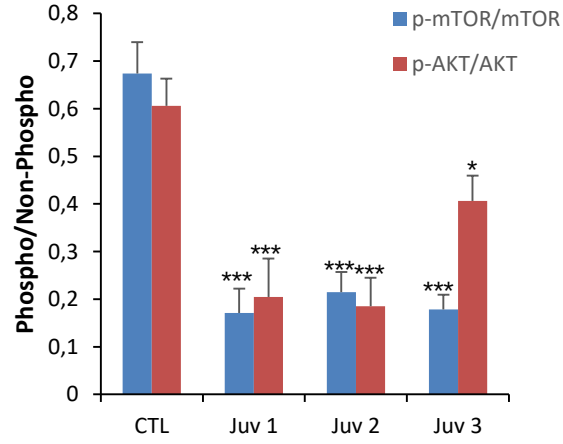
p-mTOR/mTOR
p-AKT/AKT
Phospho/Non-Phospho
0,8
0,7
0,6
0,5
0,4
0,3
0,2
0,1
0
CTL
Juv 1
Juv 2
Juv 3

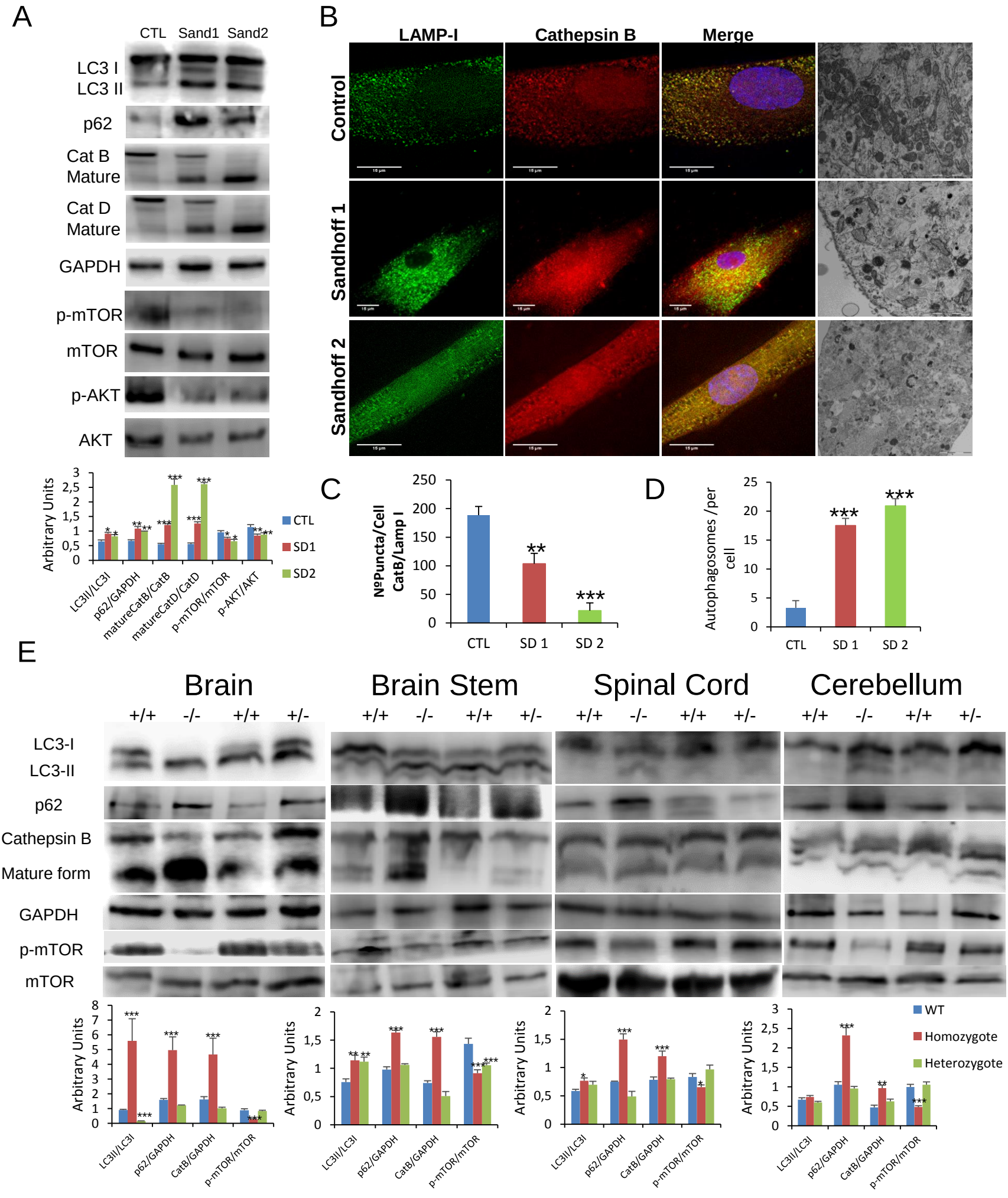
A
CTL
Sand1
Sand2
LC3 I
LC3 II
p62
Cat B
Mature
Cat D
Mature
GAPDH
p-mTOR
mTOR
p-AKT
AKT
Arbitrary Units
CTL
SD1
SD2
LC3II/LC3I
p62/GAPDH
matureCatB/CatB
matureCatD/CatD
p-mTOR/mTOR
p-AKT/AKT
B
LAMP-I
Cathepsin B
Merge
Control
Sandhoff 1
Sandhoff 2
C
NºPuncta/Cell
CatB/Lamp I
CTL
SD 1
SD 2
D
Autophagosomes /per
cell
CTL
SD 1
SD 2
E
Brain
Brain Stem
Spinal Cord
Cerebellum
+/+
-/-
+/+
+/-
LC3-I
LC3-II
p62
Cathepsin B
Mature form
GAPDH
p-mTOR
mTOR
Arbitrary Units
LC3II/LC3I
p62/GAPDH
CatB/GAPDH
p-mTOR/mTOR
WT
Homozygote
Heterozygote

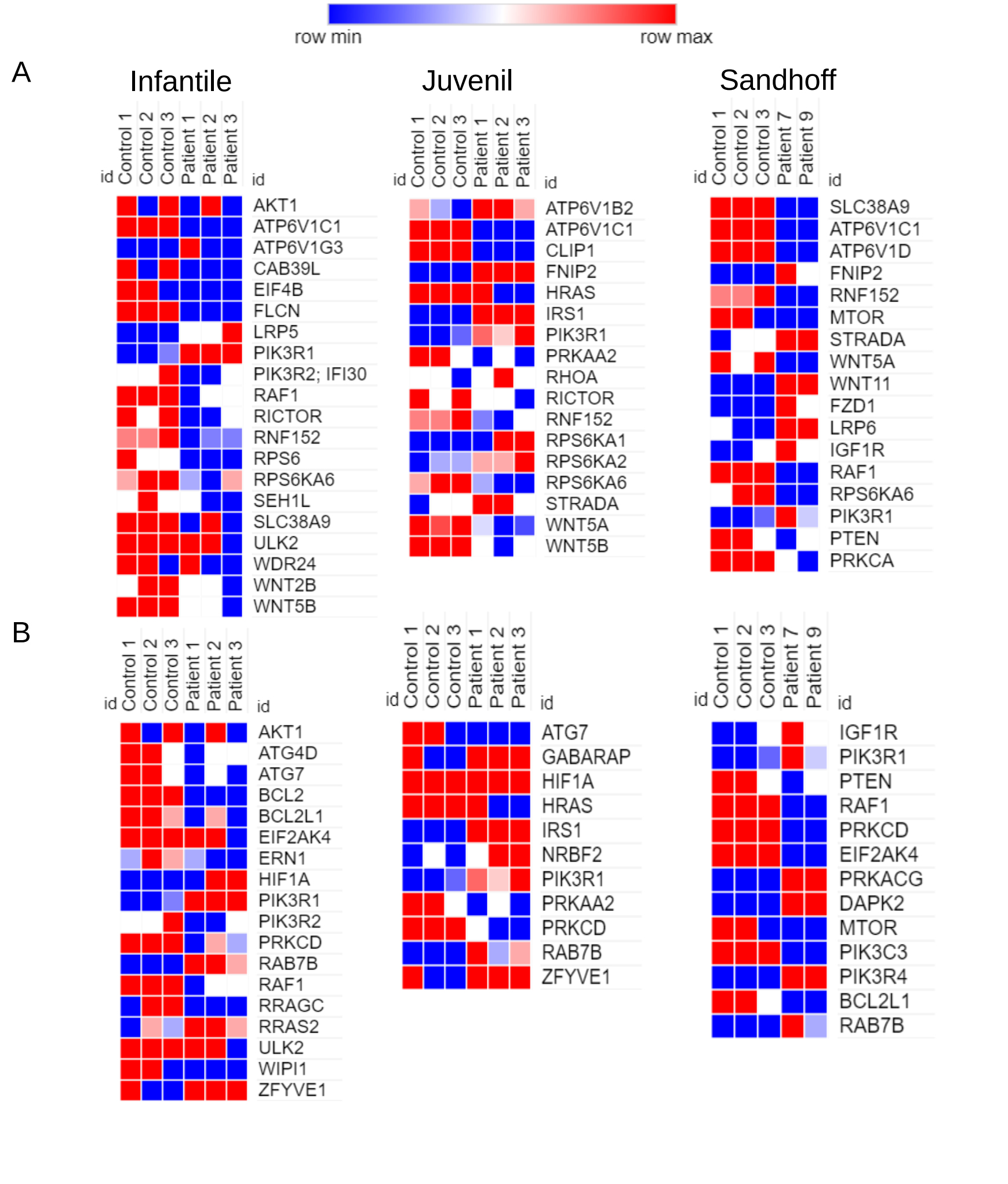
row min
row max
A
Infantile
Juvenil
Sandhoff
id
Control 1
Control 2
Control 3
Patient 1
Patient 2
Patient 3
Patient 7
Patient 9
AKT1
ATP6V1C1
ATP6V1G3
CAB39L
EIF4B
FLCN
LRP5
PIK3R1
PIK3R2; IFI30
RAF1
RICTOR
RNF152
RPS6
RPS6KA6
SEH1L
SLC38A9
ULK2
WDR24
WNT2B
WNT5B
ATP6V1B2
CLIP1
FNIP2
HRAS
IRS1
PRKAA2
RHOA
RNF152
RPS6KA1
RPS6KA2
RPS6KA6
STRADA
WNT5A
WNT5B
ATP6V1D
MTOR
STRADA
WNT5A
WNT11
FZD1
LRP6
IGF1R
PTEN
PRKCA
B
ATG4D
ATG7
BCL2
BCL2L1
EIF2AK4
ERN1
HIF1A
PIK3R2
PRKCD
RAB7B
RRAGC
RRAS2
WIPI1
ZFYVE1
GABARAP
NRBF2
PRKCA
PRKCD
PRKACG
DAPK2
PIK3C3
PIK3R4

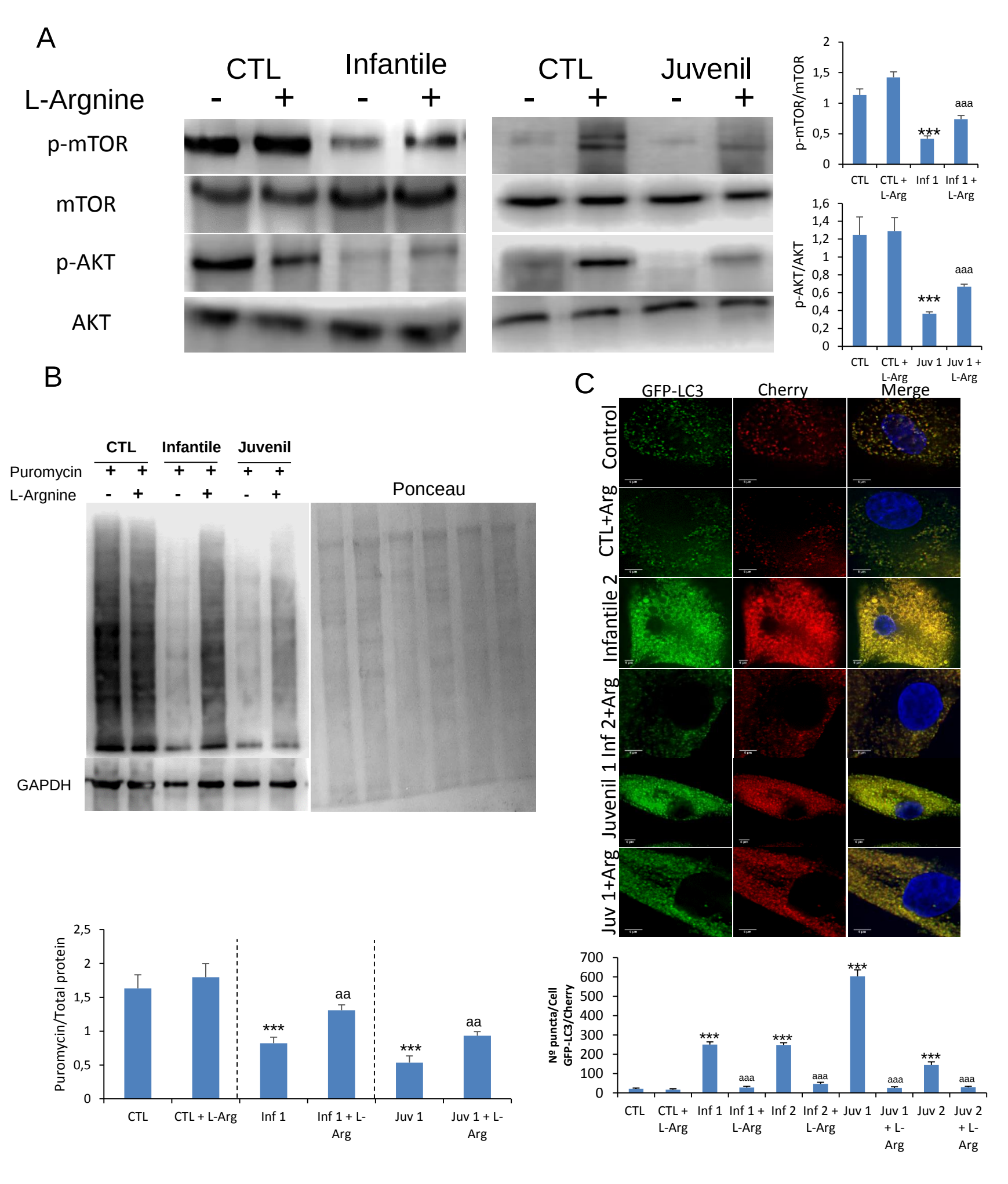
A
CTL
Infantile
CTL
Juvenil
L-Argnine
- + - + - + - +
p-mTOR
mTOR
p-AKT
AKT
p-mTOR/mTOR
2
1,5
1
0,5
0
***
aaa
CTL
CTL + L-Arg
Inf 1
Inf 1 + L-Arg
p-AKT/AKT
1,6
1,4
1,2
1
0,8
0,6
0,4
0,2
0
***
aaa
CTL
CTL + L-Arg
Juv 1
Juv 1 + L-Arg
B
CTL
Infantile
Juvenil
Puromycin
+ + + + + +
L-Argnine
- + - + - +
Ponceau
GAPDH
Puromycin/Total protein
2,5
2
1,5
1
0,5
0
***
aa
***
aa
CTL
CTL + L-Arg
Inf 1
Inf 1 + L-Arg
Juv 1
Juv 1 + L-Arg
C
GFP-LC3
Cherry
Merge
Control
CTL+Arg
Infantile 2
Juvenil 1 Inf 2+Arg
Juv 1+Arg
Nº puncta/Cell GFP-LC3/Cherry
700
600
500
400
300
200
100
0
***
***
***
***
aaa
aaa
aaa
aaa
CTL
CTL + L-Arg
Inf 1
Inf 1 + L-Arg
Inf 2
Inf 2 + L-Arg
Juv 1
Juv 1 + L-Arg
Juv 2
Juv 2 + L-Arg

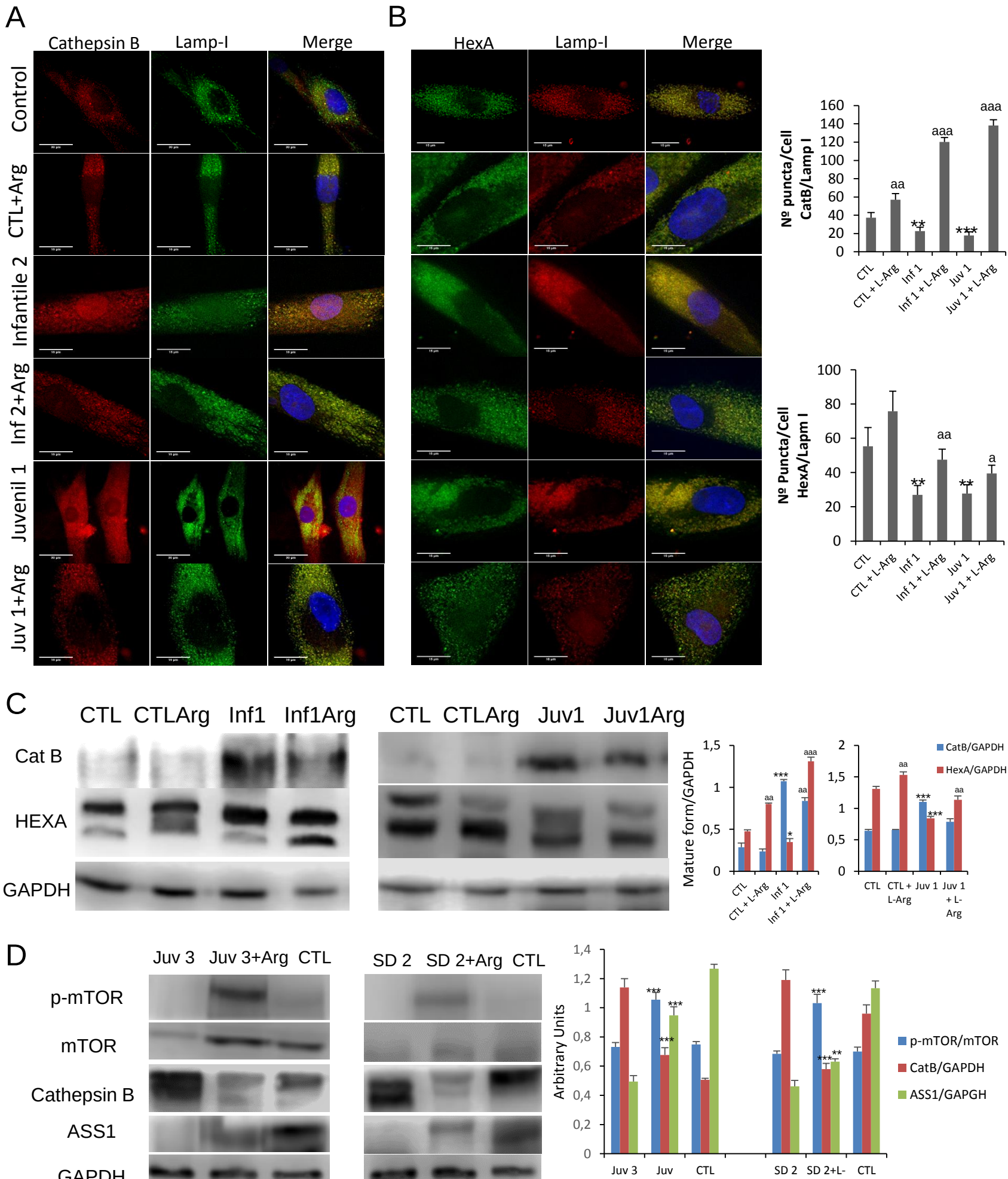
A
Cathepsin B
Lamp-I
Merge
Control
CTL+Arg
Infantile 2
Inf 2+Arg
Juvenil 1
Juv 1+Arg
B
HexA
Lamp-I
Merge
Nº puncta/Cell CatB/Lamp I
CTL
CTL + L-Arg
Inf 1
Inf 1 + L-Arg
Juv 1
Juv 1 + L-Arg
Nº Puncta/Cell HexA/Lapm I
C
CTL CTLArg Inf1 Inf1Arg
CTL CTLArg Juv1 Juv1Arg
Cat B
HEXA
GAPDH
Mature form/GAPDH
CatB/GAPDH
HexA/GAPDH
D
Juv 3 Juv 3+Arg CTL
SD 2 SD 2+Arg CTL
p-mTOR
mTOR
Cathepsin B
ASS1
GAPDH
Arbitrary Units
p-mTOR/mTOR
CatB/GAPDH
ASS1/GAPGH
Juv 3
Juv 3+L-Arg
CTL
SD 2
SD 2+L-Arg
CTL

Supplementary data

L-arginine ameliorates defective autophagy in GM2 gangliosidoses by mTOR modulation

Beatriz Castejón-Vega[1], Débora Lendines-Cordero[1], Alejandro Rubio[2], Antonio J. Pérez-Pulido[2], Pedro Bullón[1], José L. Quiles[3], Jon D. Lane[4], Beatriz Fernández-Domínguez[5], María Begoña Cachón-González[6], Carmen Martín-Ruiz[7], Alberto Sanz[8], Timothy M. Cox[6], Elísabet Alcocer-Gómez[9], Mario D. Cordero[10]

[1] Research Laboratory, Oral Medicine Department, University of Sevilla, Sevilla, Spain

[2] Centro Andaluz de Biologia del Desarrollo (CABD, UPO-CSIC-JA). Facultad de Ciencias Experimentales (Área de Genética), Universidad Pablo de Olavide, 41013, Sevilla, Spain.

[3] Department of Physiology, Institute of Nutrition and Food Technology "José Mataix Verdú", Biomedical Research Center, University of Granada, Granada, Spain.

[4] Cell Biology Laboratories, School of Biochemistry, University of Bristol, Bristol, UK

[5]Acción y Cura para Tay-Sachs (ACTAYS), Madrid, Spain

[6] Department of Medicine, University of Cambridge, Cambridge, UK.

[7] Biosciences Institute, Newcastle University, Newcastle upon Tyne, UK.

[8]Institute of Molecular, Cell and Systems Biology, University of Glasgow, Glasgow G12 8QQ, UK.

[9] Departamento de Psicología Experimental, Facultad de Psicología, Universidad de Sevilla, Seville Spain.

[10] Instituto de Investigación e Innovación en Ciencias Biomédicas de Cádiz (INiBICA), Cadiz, Spain.

Running Title: Disrupted autophagy and mTOR in Tay-Sachs disease.

Corresponding Authors:

Dr. Mario D. Cordero
Instituto de Investigación e Innovación en Ciencias Biomédicas de Cádiz (INiBICA), Cadiz, Spain, Email: mario.cordero@inibica.es

Supplementary Table 1. Clinical characteristic of the patients

Infantile 1	
2 years old	Gender: Male
Signs and symptoms:	
-Epilepsy	-Startle with noise
-Abnormal ocular movements	- Hyperreflexia
-Respiratory problems	-Psychomotor regression
-Macrocephaly	-Low visual acuity
-Hypotonia severe	-Pyramidal syndrome
Enzyme levels:	
-Isoenzymatic distribution %A: 33,5%	RL: 84,0-97,0
-Isoenzymatic distribution %B: 66,5%	RL: 3,0-16,0
-β-hexosaminidase total: 1916 nmol/h/mg prot	RL:336-2868
-β-hexosaminidase A: 4 nmol/h/mg prot	RL:61-316
-Esfingomielinase: 14,9 nmol/17h/mg prot	RL:8,5-26,0
-β-glucocerebrosidase: 14,6 nmol/h/mg prot	RL:2,9-27,6
Infantile 2	
1 year old	Gender: Male
Signs and symptoms:	
-Startle with noise	-Abnormal ocular movements
-Absent of cephalic support	-Hyperreflexia
-Psychomotor delays	-Cherry-red spot
-Respiratory problems	-Dysphagia
-Severe hypotonia	
Biochemistry: -CPK, CDT, iron metabolism, folic acid, B12 vitamin, lactate, ammonium, copper, ceruloplasmina, immunoglobulins, homocysteine, 3-hydroxybutyrate, free fatty acids, long-chain fatty acids: Normal levels	
Very low HexA enzymatic activity	
Infantile 3	
4 years old	Gender: Female
Signs and symptoms:	
-Macrocephaly	-Absence of cephalic support
-Visual deficit	-Epilepsies
-Total absence of the language	-Muscle spams
-Hipotonia	-Cherry-red spot
-Absence of autonomous displacement	-Hipomielynization
Biochemistry: -CPK, CDT, folic acid, B12 vitamin, lactate, ammonium, copper, ceruloplasmina, immunoglobulins, homocysteine, 3-hydroxybutyrate, free fatty acids, long-chain fatty acids: Normal levels	
Very low HexA enzymatic activity	
Juvenile 1	
14 years old	Gender: Male

Signs and symptoms:

-Development delays
-Startle with noise
-Facial dysmorphia
-Macrocephaly
-Slight psychomotor development delay
-Drops-attacks episodes
-Motor and language regression
-Dysphagia
-Myelination alteration
-Slow brain activity
-Visual deficit

Biochemistry:

-Low levels of HDL
-High levels of AST and LDH
-Lactate, ammonium, amino acids, iron profile, creatine, guanidinoacetate, organic acids, GAGs, 4-OH butyrate: Normal levels

Low levels of HexA activity: 3nmol/h/mg prot RL: 61-316 3nmol/h/mg prot

Juvenile 2

13 years old Gender: Female

Signs and symptoms:

-Severe dysphagia
-Motor delays
-Language regression (skills)
-Skills and motor regression
-Somatocraneal disproportion
-Slow movements
-Cherry-red spot

Biochemistry:

-CPK, ammonium, lactate, ceruloplasmin, iron profile, B12 vitamin, folic acid, amino acids, long-chain fatty acids: Normal levels

Low levels of HexA

Juvenile 3

16 years old Gender: Female

Sings and symptoms:

-Language regression
-Dysphagia
-Dysarthria
-Motor delays
-Lumbar hyperlodosis

Low HexA enzymatic activity 6% of activity

65% of discapacity

Supplementary Table 2. Genetic characteristic of the patients.

Patient	Nº Alelle	Mutation	Affects Stability?	Affects active site?
Infantile 1	Alelle 1	Premature STOP codon	Yes	Yes
	Alelle 2	Splicing	Unknown	Unknown
Infantile 2	Alelle 1	Near splicing site	Unknown	Unknown
	Alelle 2	Near splicing site	Unknown	Unknown
Infantile 3	Alelle 1	Near splicing site	Unknown	Unknown
	Alelle 2	Near splicing site	Unknown	Unknown
Juvenil 1	Alelle 1	Point	No	No
	Alelle 2	Point	Yes	Yes
Juvenil 2	Alelle 1	Point	Yes	Yes
	Alelle 2	Point	Unknown	Unknown
Juvenil 3	Alelle 1	Splicing	Unknown	Unknown
	Alelle 2	Point (Synonymous substitution)	No	No
Sandhoff 1	Alelle 1	Point	Yes	No
	Alelle 2	Intron	No	No
Sandhoff 2	Alelle 1	Premature STOP codon	Yes	Yes
	Alelle 2	Intron	No	No

Supplementary Table 3. Significant changes in mTOR pathway genes in patients *vs* control (ANOVA p-value <0.05, >1.5 fold).

Juvenile			
Gene Symbol	**Fold-Change**	**ANOVA p-value**	**Gene IDs**
PIK3R1	12,94	0,001497	NM_001242466
RPS6KA2	3,23	0,01184	NM_001006932
ATP6V1B2	2,84	0,035385	NM_001693
FNIP2	2,39	0,007737	NM_020840
RPS6KA1	1,69	0,044762	ENST00000627677
IRS1	1,55	0,031457	NM_005544
CLIP1	-1,49	0,01208	NM_001247997
HRAS	-1,72	0,035889	NM_005343
ATP6V1C1	-1,73	0,02705	NM_001695
RICTOR	-1,91	0,0558	NM_001285439
PRKAA2	-2,71	0,040698	NM_006252
WNT5B	-2,85	0,022171	NM_030775
RPS6KA6	-4,34	0,007977	NM_014496
RNF152	-6,08	0,009278	NM_173557
WNT5A	-47,42	0,003877	NM_001256105
Infantile			
Gene Symbol	**Fold-Change**	**ANOVA p-value**	**Gene IDs**
PIK3R1	12,95	2,06E-05	NM_001242466
LRP5	3,81	0,0045	NM_001291902
RPS6KA2	2,51	0,0337	NM_001006932
FNIP2	2,12	0,0207	NM_020840
LRP6	2,04	0,0392	ENST00000628182
ATP6V1E2	2,03	0,043	NM_080653
WNT11	2	0,0283	NM_004626
ATP6V1B2	1,93	0,0207	NM_001693
TNFRSF1A	1,88	0,0197	NM_001065
EIF4E2	1,86	0,0489	NM_001276336
FZD1	1,84	0,0387	NM_003505
NPRL3	1,79	0,0382	NM_001039476
ATP6V1G3	1,54	0,0105	NM_133262
FZD5	-1,48	0,0182	NM_003468
SLC38A9	-1,55	0,0502	NM_001258286
RAF1	-1,78	0,0051	NM_002880
ATP6V1C1	-1,83	0,0037	NM_001695
AKT1	-1,89	0,0477	NM_001014431
WNT2B	-1,95	0,0126	NM_001291880
PIK3R2; IFI30	-2,01	0,0325	NM_005027
PRKAA2	-2,03	0,0205	NM_006252

SEH1L	-2,33	0,0121	NM_001013437
IGF2; INS-IGF2	-2,46	0,0003	NM_001007139
WNT5B	-2,74	0,015	NM_030775
RPS6KA6	-2,8	0,0027	NM_014496
RICTOR	-2,83	0,0018	NM_001285439
LPIN1; MIR548S	-4,22	0,0083	NM_001261427
RNF152	-8,06	6,21E-06	NM_173557
Sandhoff			
Gene Symbol	**Fold-Change**	**ANOVA p-value**	**Gene IDs**
PIK3R1	10,84	0,038841	NM_001242466
FNIP2	3,05	0,013828	NM_020840
STRADA	2,31	0,028354	NM_001003786
LRP6	2,02	0,00027	NM_002336
IGF1R	1,95	0,034823	NM_000875
ATP6V1C1	-1,64	0,044767	NM_001695
RAF1	-1,74	0,036988	NM_002880
PRKCA	-2,95	0,020134	NM_002737
RPS6KA6	-3	0,017731	NM_014496
WNT5A	-3,91	0,026136	NM_001256105
RNF152	-10,18	0,007434	NM_173557

Supplementary Table 4. Significant changes in Autophagy pathway genes in patients *vs* control (ANOVA p-value <0.05, >1.5 fold).

Infantile			
Gene Symbol	**Fold-Change**	**ANOVA p-value**	**Gene IDs**
PIK3R1	12,95	2,06E-05	NM_001242466
RAB7B	5,1	0,0001	NM_001164522
RRAS2	3,31	0,0022	NM_001102669
DAPK1	2,26	0,0281	NM_001288729
ZFYVE1	2,05	0,0204	NM_001281734
HIF1A	2,03	0,0277	NM_001243084
GABARAP	1,87	0,0073	NM_007278
BAD	1,84	0,0049	NM_004322
CTSB	1,72	0,034	NM_001908
ATG10	1,64	0,0259	NM_001131028
RAF1	-1,78	0,0051	NM_002880
AKT1	-1,89	0,0477	NM_001014431
PIK3R2; IFI30	-2,01	0,0325	NM_005027
PRKAA2	-2,03	0,0205	NM_006252
ATG4D	-2,17	0,0145	NM_001281504
IGF2; INS-IGF2	-2,46	0,0003	NM_001007139
ATG7	-2,7	0,0022	NM_001136031
ERN1	-3,29	0,0032	NM_001433
PRKCD	-3,64	0,0003	NM_006254
Juvenile			
Gene Symbol	**Fold-Change**	**ANOVA p-value**	**Gene IDs**
PIK3R1	12,94	0,001497	NM_001242466
RAB7B	2,87	0,01827	NM_001164522
GABARAP	1,92	0,031715	NM_007278
HIF1A	1,72	0,01766	NM_001243084
ZFYVE1	1,71	0,04872	NM_001281734
IRS1	1,55	0,031457	NM_005544
HRAS	-1,72	0,035889	NM_005343
PRKCD	-2,28	0,024094	NM_006254
PRKAA2	-2,71	0,040698	NM_006252

Sandhoff			
Gene Symbol	**Fold-Change**	**ANOVA p-value**	**Gene IDs**
PIK3R1	10,84	0,038841	NM_001242466
RAB7B	3,68	0,042686	NM_001164522
IGF1R	1,95	0,034823	NM_000875
DAPK2	1,92	0,019391	NM_014326
PRKACG	1,83	0,0003	NM_002732
PIK3R4	1,63	0,037854	NM_014602
PIK3CD	-1,38	0,00897	NM_005026
VAMP8	-1,43	0,042707	NM_003761
PIK3C3	-1,62	0,039853	NM_001308020
RAF1	-1,74	0,036988	NM_002880
EIF2AK4	-1,88	0,016362	NM_001013703
BCL2L1	-3,26	0,011985	NM_001191
PRKCD	-3,6	0,005909	NM_006254

Supplementary Table 5. Significant changes in lysosome pathway genes in patients *vs* control (ANOVA p-value <0.05, >1.5 fold).

Juvenile			
Gene Symbol	**Fold-Change**	**ANOVA p-value**	**Gene IDs**
CD68	4,16	0,040966	NM_001040059
CTSO	2,68	0,037234	NM_001334
LAPTM4A	1,8	0,020544	hsa_circ_0000981
IGF2R	-1,58	0,022001	NM_000876
LITAF	-1,7	0,021841	NM_001136472
SCARB2	-1,88	0,009984	NM_001204255
NAGA	-2,18	0,021429	NM_000262
CLTCL1	-2,37	0,037322	NM_001835
NEU1	-2,57	0,048515	ENST00000375631
CTSZ	-2,82	0,030783	NM_001336
AGA	-3,03	0,044367	NM_000027
ARSG	-4,12	0,037029	NM_001267727
NPC1	-5,83	0,031279	NM_000271
SORT1	-5,89	0,010414	NM_001205228
Infatile			
Gene Symbol	**Fold-Change**	**ANOVA p-value**	**Gene IDs**
CD68	5,7	0,036	NM_001040059
CTSO	2	0,0252	NM_001334
ARSA	1,9	0,0356	NM_000487
CTSB	1,72	0,034	NM_001908
LGMN	1,62	0,0414	NM_001008530
CTSF	1,49	0,0346	NM_003793
LAPTM4B	-1,87	0,0051	NM_018407
LIPA	-2,19	0,0152	NM_000235
NEU1	-2,75	0,0067	ENST00000375631
CTNS	-2,81	0,0057	NM_001031681
AGA	-3,45	0,0006	NM_000027
ARSG	-3,52	0,0172	NM_001267727
NPC1	-7,34	0,0004	NM_000271
HEXA	-27,12	0,0075	NM_000520
Sandhoff			
Gene Symbol	**Fold-Change**	**ANOVA p-value**	**Gene IDs**
CD68	7,3	0,003732	NM_001040059
LAPTM4A	2,51	0,044028	hsa_circ_0000981
AP1G2	1,2	0,026778	NM_001282474
CLTC	-1,33	0,034873	NM_001288653
CLTA	-1,35	0,000585	NM_001076677
LITAF	-2,34	0,006126	NM_001136472
IGF2R	-2,36	0,027342	NM_000876

AGA	-3,51	0,008182	NM_000027

Supplementary Table 6. Significant changes in arginine biosynthesis pathway genes in patients *vs* control (ANOVA p-value <0.05, >1.5 fold).

Juvenile			
Gene Symbol	**Fold-Change**	**ANOVA p-value**	**Gene IDs**
CPS1	1,96	0,040666	NM_001122633
ABHD14A-ACY1	1,69	0,003892	OTTHUMT00000349691
GOT2	-3,89	0,032579	NM_001286220
GLUL	-4,21	0,003389	NM_001033044
ASS1	-12,13	0,002704	NM_000050

Infantile			
Gene Symbol	**Fold-Change**	**ANOVA p-value**	**Gene IDs**
GLS	3,03	0,018	NM_001256310
GOT1	-1,5	0,0427	NM_002079
NOS3	-1,71	0,0237	NOS3.kAug10-unspliced
GOT2	-3,71	0,0113	NM_001286220
GLUL	-5,81	6,62E-06	NM_001033044
ASS1	-8,45	0,0003	NM_000050

Sandhoff			
Gene Symbol	**Fold-Change**	**ANOVA p-value**	**Gene IDs**
ABHD14A-ACY1	2	0,005936	OTTHUMT00000349691
GOT2	-4,04	0,040265	NM_001286220
GLUL	-4,56	0,009998	NM_001033044
ASS1	-44,73	0,013876	NM_000050

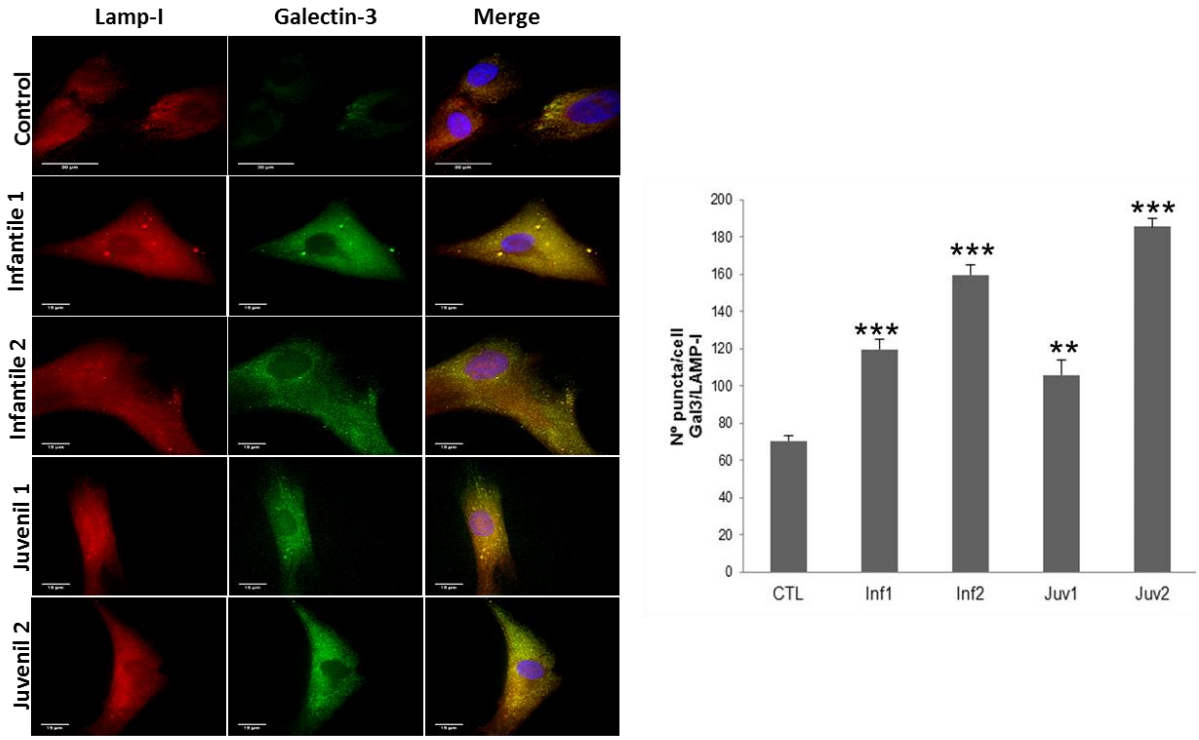

Supplementary Figure 1. Representative fluorescence images and quantification of fibroblasts from control and TSD. Cells were fixed and stained with anti-Galectin-3 antibodies (green) and anti-LAMP-I (red). Nuclei were stained with Hoechst 33342 (blue). Increased Galectin-3- puncta and colocalization of Galectin-3 and LAMP-I puncta are shown in patients. The data are the mean ± SD for experiments conducted on 2 different control cell lines and three separate experiments. ***$p < 0.001$, **$p < 0.005$, *$p < 0.05$ between controls and TSD patients.

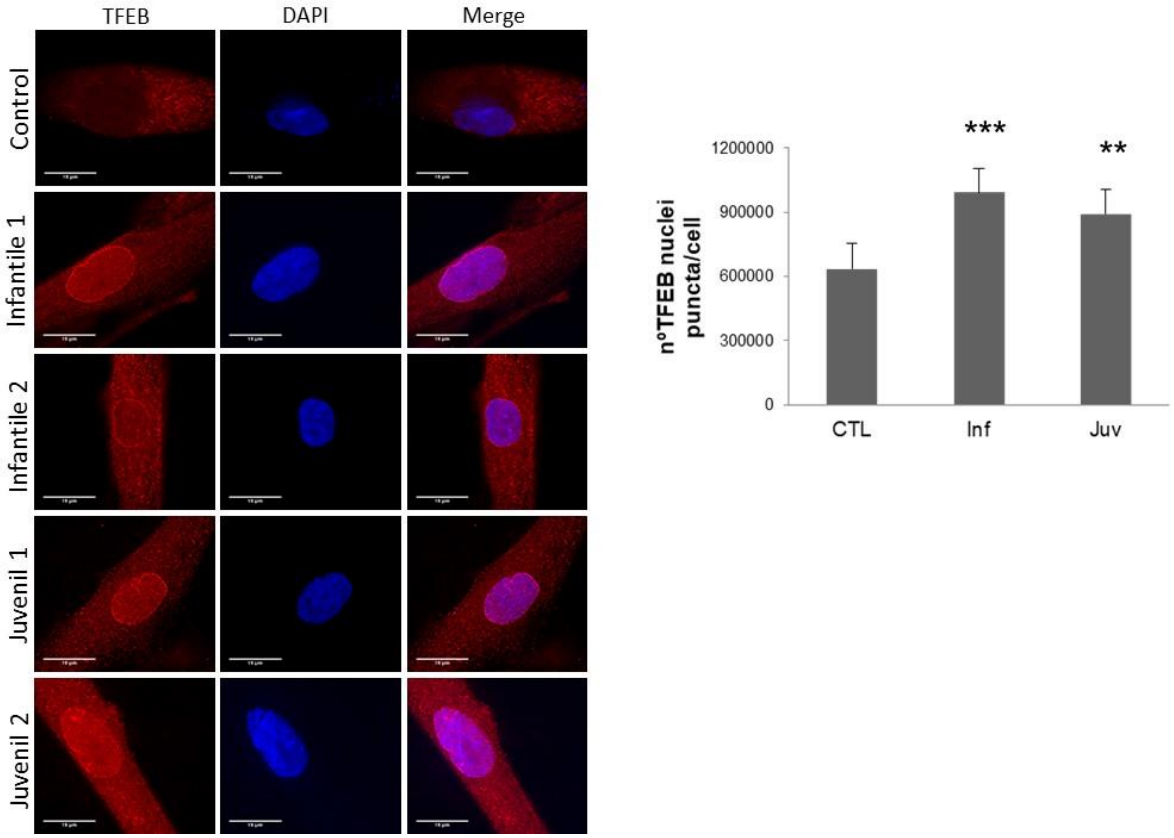

Supplementary Figure 2. Representative fluorescence images and quantification of fibroblasts from control and Tay-Sachs (TSD). Cells were fixed and stained with anti-TFEB antibodies (red). Nuclei were stained with Hoechst 33342 (blue). Increased TFEB in nucleus are shown in patients by red and blue fluorescence signal colocalization.

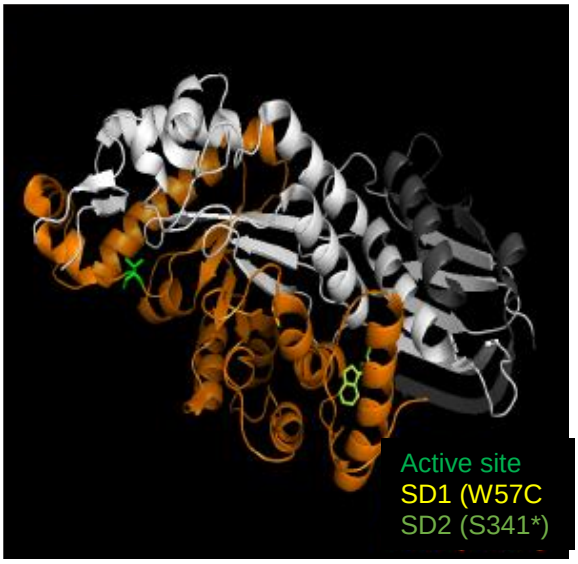

Supplementary Figure 3. HEXB point mutations and frameshifts. The active site is also highlighted. Grey colour represents the propeptide, and white colour represents the main chain of the protein. Orange color represents the sequence lost by the SD1 patient due to a frameshift.

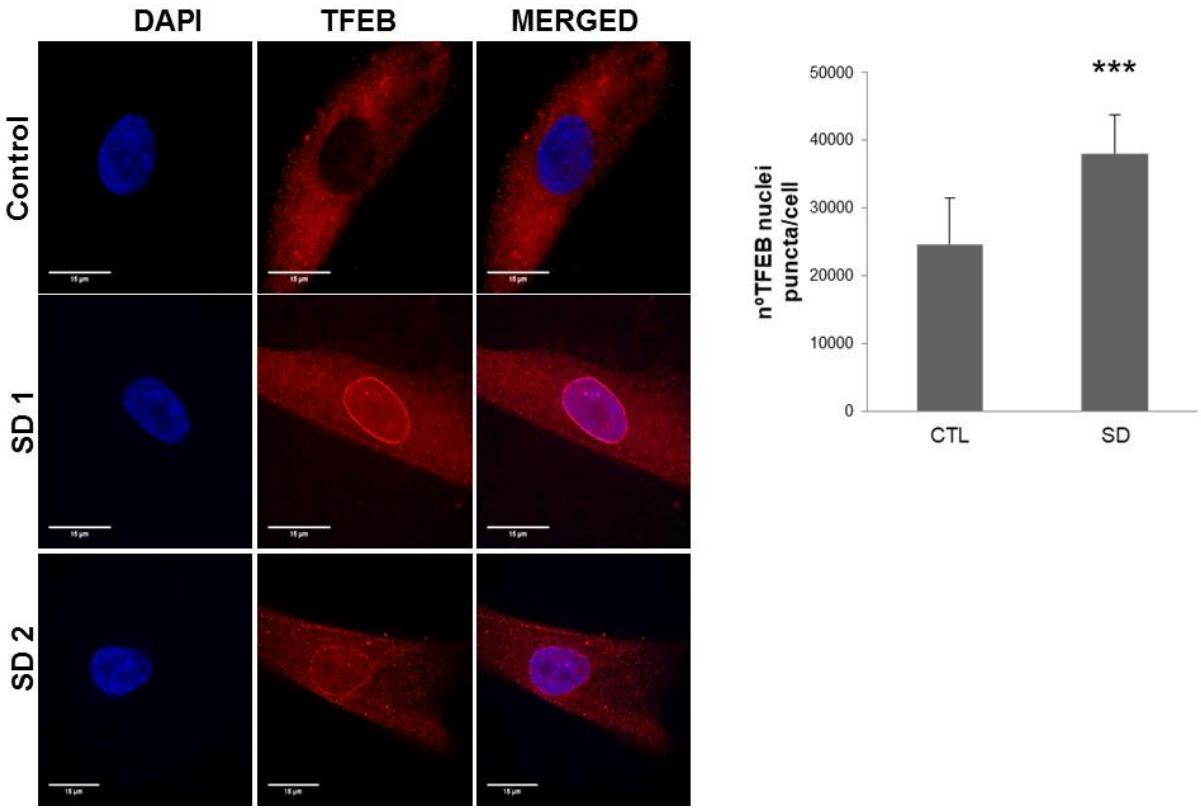

Supplementary Figure 4. Representative fluorescence images and quantification of fibroblasts from control and Sandhoff (SD). Cells were fixed and stained with anti-TFEB antibodies (red). Nuclei were stained with Hoechst 33342 (blue). Increased TFEB in nucleus are shown in patients by red and blue fluorescence signal colocalization.

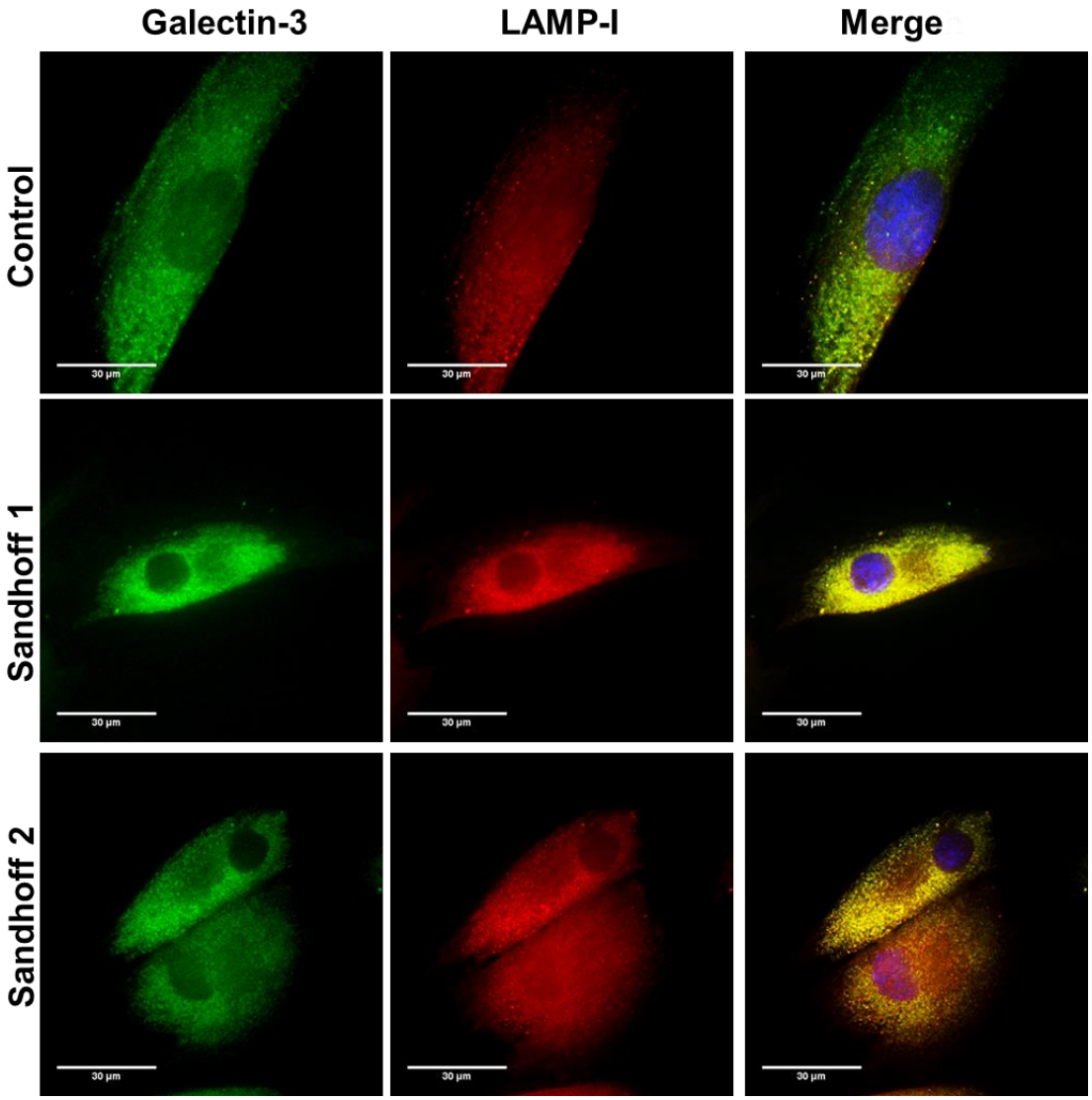

Supplementary Figure 5. Representative fluorescence images and quantification of fibroblasts from control and Sandhoff patients. Cells were fixed and stained with anti-Galectin-3 antibodies (green) and anti-LAMP-I (red). Nuclei were stained with Hoechst 33342 (blue).

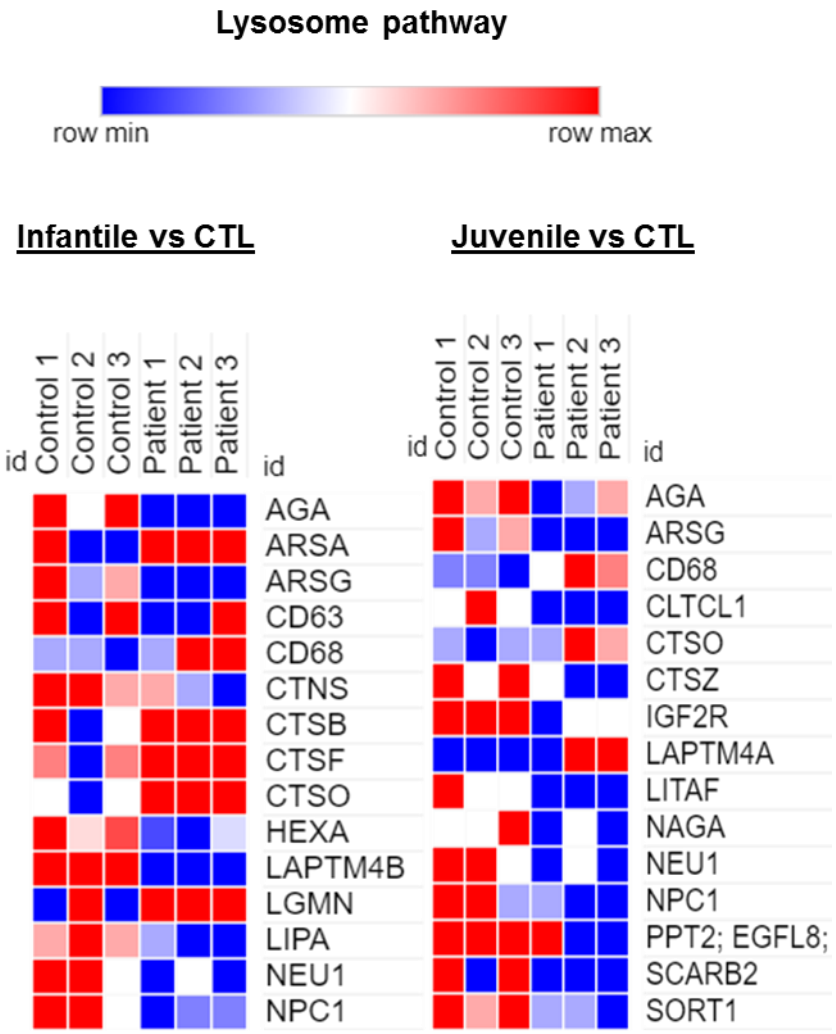

Supplementary Figure 6. Heatmap clustering of enrichment (z-scores) of the lysosome function in set of coding genes differentially expressed between Control vs Tay-Sachs patients (n = 3 per case).

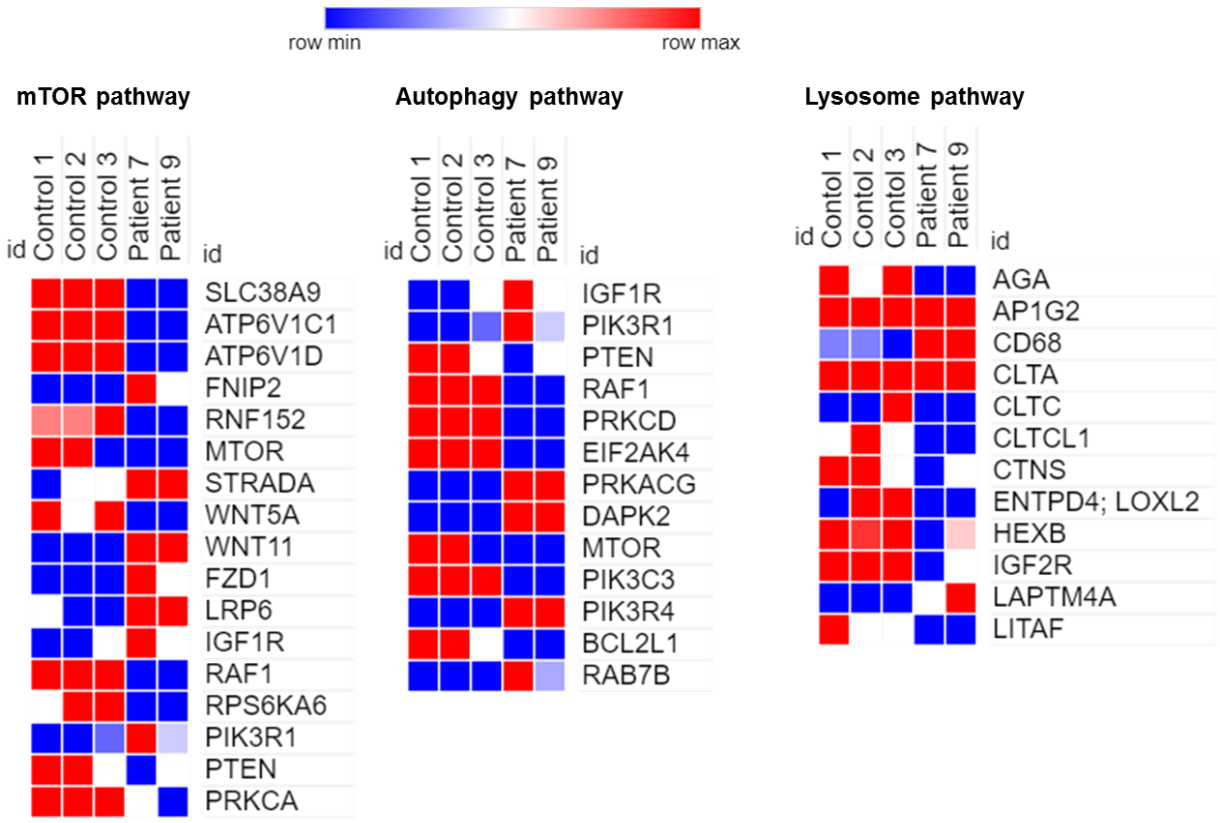

Supplementary Figure 7. Heatmap clustering of enrichment (z-scores) of the mTOR (left), autophagy (center) and lysosome (right) functions in set of coding genes differentially expressed between Control vs Sandhoff patients (n = 3 per case).

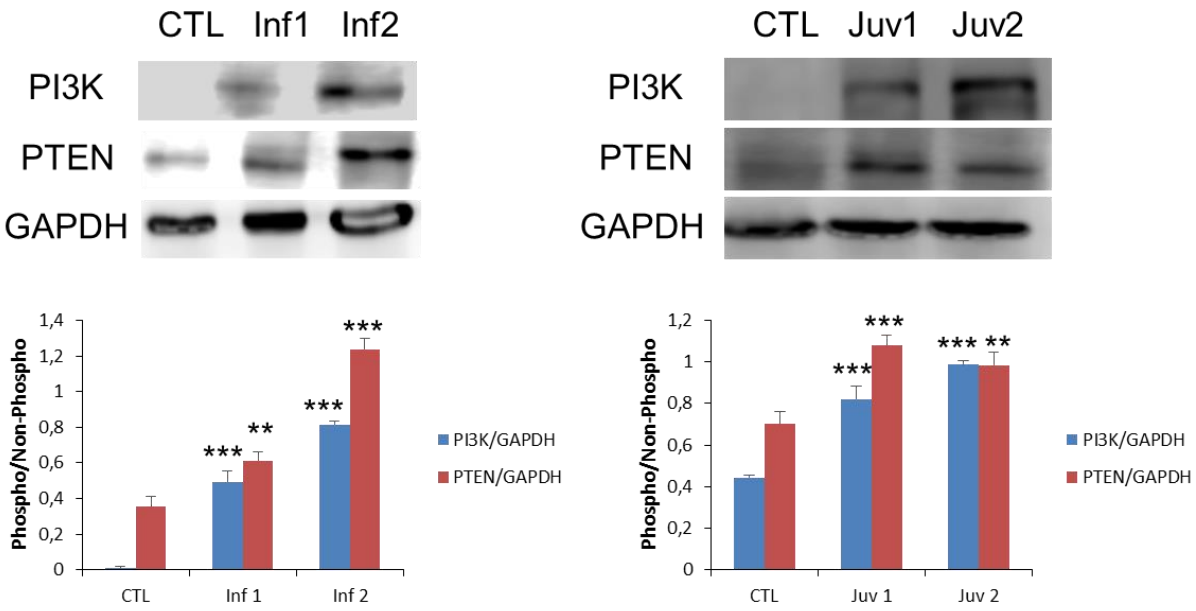

Supplementary Figure 8. Protein expression levels of PI3K and PTEN of representative control and Tay-Sachs patient fibroblasts. The data are the mean ± SD for experiments conducted on 2 different control cell lines and three separate experiments. *P < 0.05; **P < 0.01; ***P < 0.001 between control and patients.

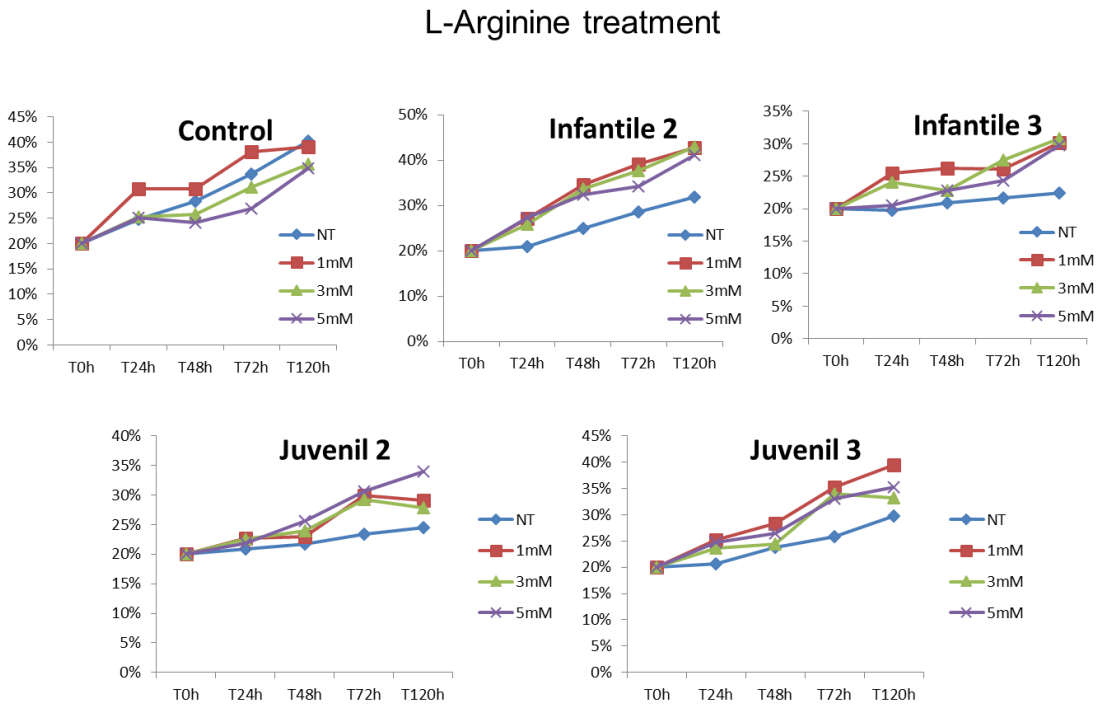

Supplementary Figure 9. Percentage of cell growth with L-Arginine determined in healthy and representative Tay-Sachs fibroblasts using three different doses (1, 3 and 5mM).

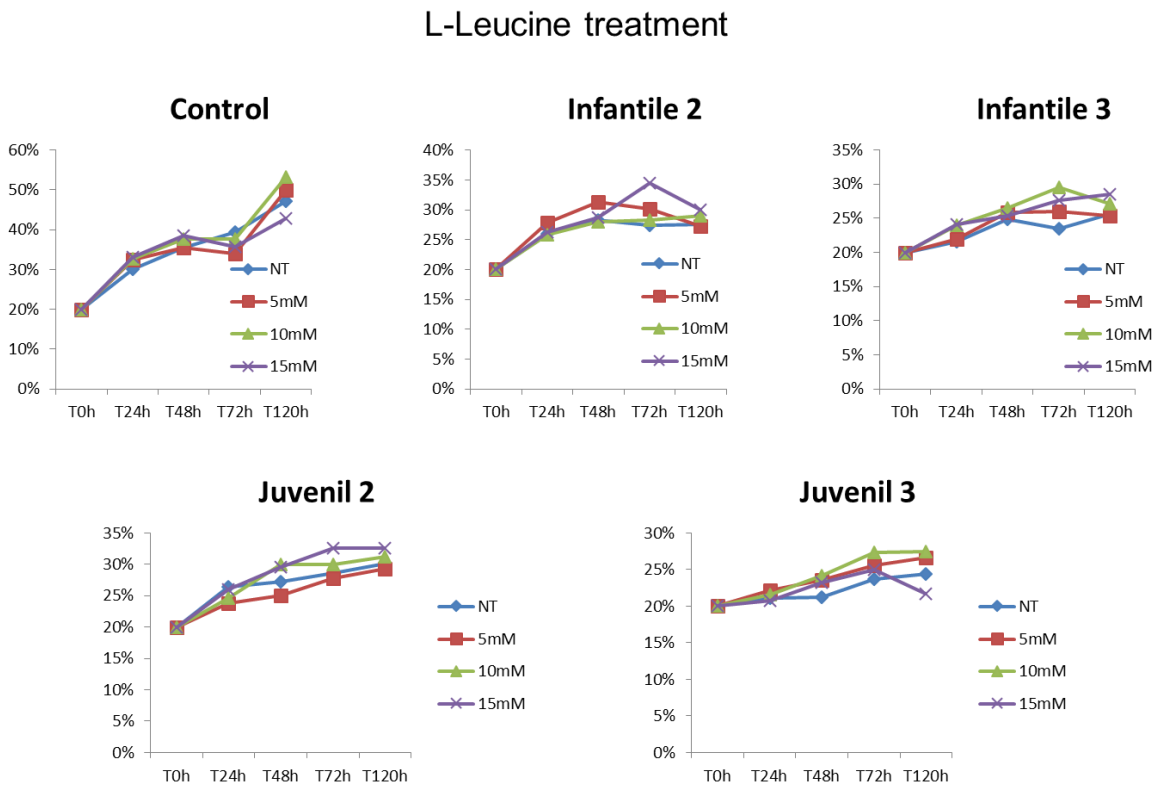

Supplementary Figure 10. Percentage of cell growth with L-Leucine determined in healthy and representative Tay-Sachs fibroblasts using three different doses (5, 10 and 15mM).

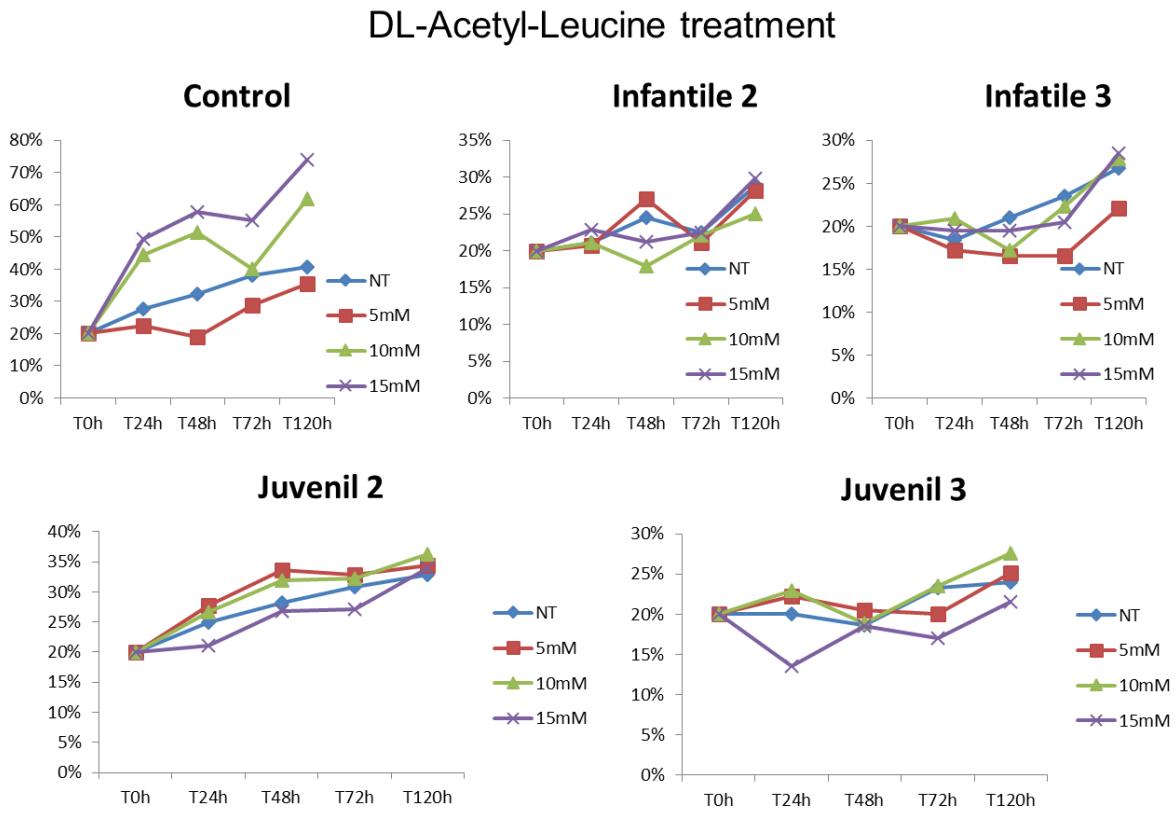

Supplementary Figure 11. Percentage of cell growth with DL-Acetyl-Leucine determined in healthy and representative Tay-Sachs fibroblasts using three different doses (5, 10 and 15mM).

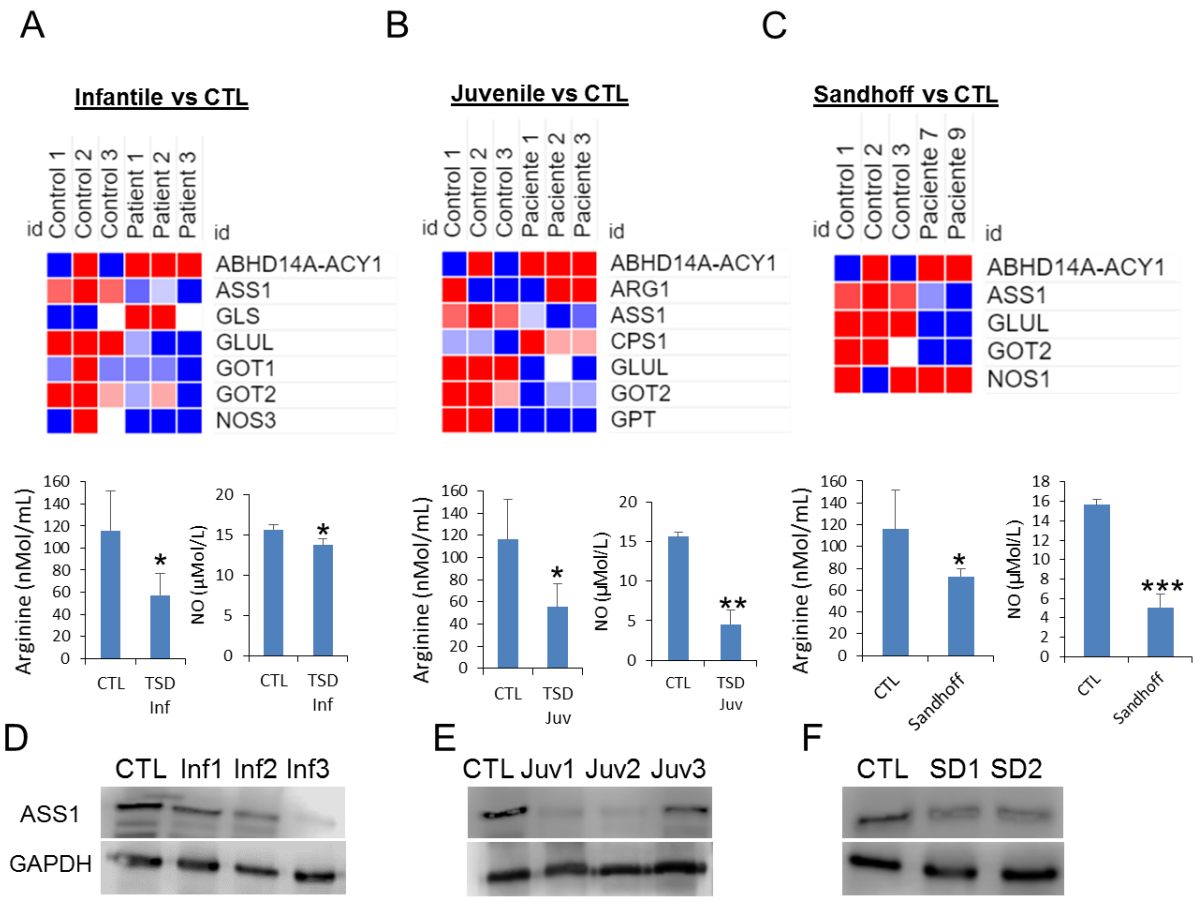

Supplementary Figure 12. Heatmap clustering of enrichment (z-scores) of the arginine biosynthesis functions in set of coding genes differentially expressed and serum arginine and nitric oxide levels in infantile Tay-Sachs (TSD) (A), juvenil TSD (B) and Sandhoff (SD) (C) (n = 3 per case). Protein expression levels of ASS1 in fibroblasts from infantile TSD (D), juvenil TSD (E) and SD (F). The data are the mean ± SD for experiments conducted on 2 different control cell lines and three separate experiments. *P < 0.05; **P < 0.01; ***P < 0.001 between control and patients;

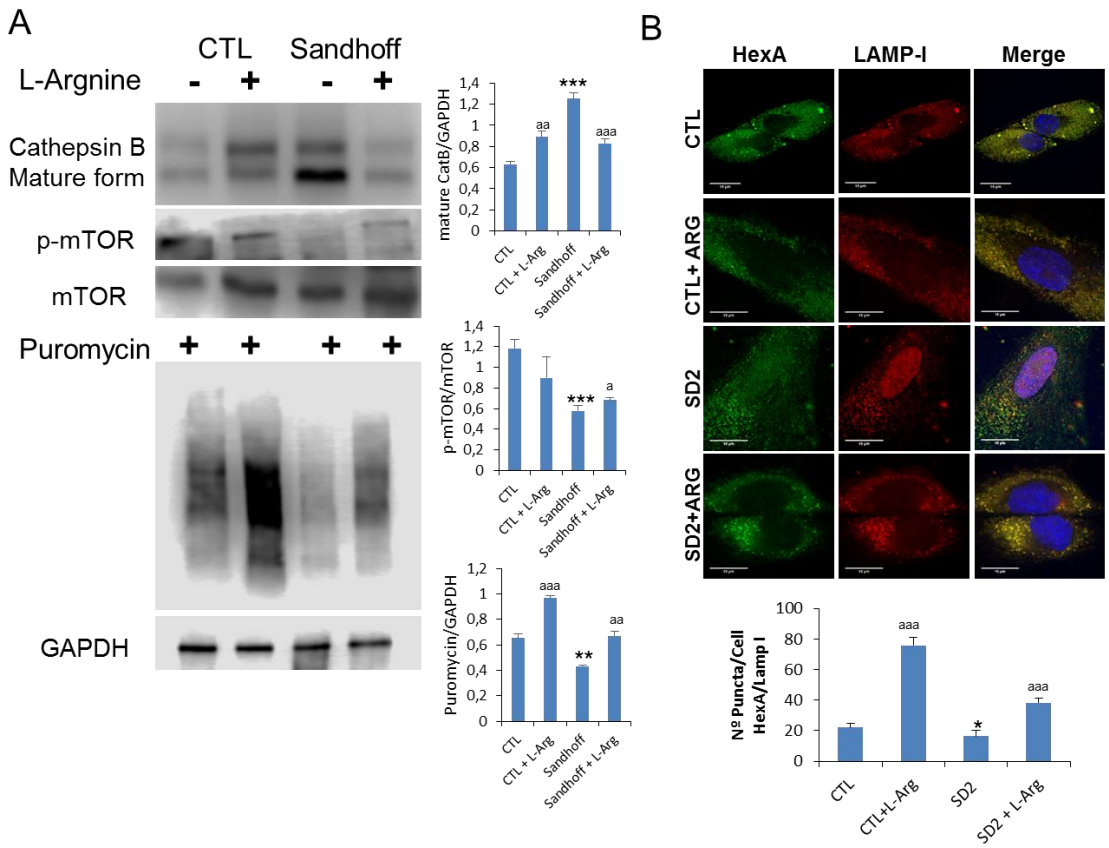

Supplementary Figure 13. A. Protein expression levels of mTOR and CatB were determined in control and representative SD fibroblast cultures after l-arginine treatment (120h). Protein synthesis was quantified in protein extracts of control and Sandhoff (SD) fibroblasts treated with l-arginine using puromycin labeling followed by immunoblot. B. Immunofluorescence of HexA in control and SD cells and quantification after l-arginine treatment. The data are the mean ± SD for experiments conducted on 2 different control cell lines and three separate experiments. *P < 0.05; **P < 0.01; ***P < 0.001 between control and SD patients; [a] P < 0.05; [aa] P < 0.01; [aaa] P < 0.001 between non-treated and treated cells.

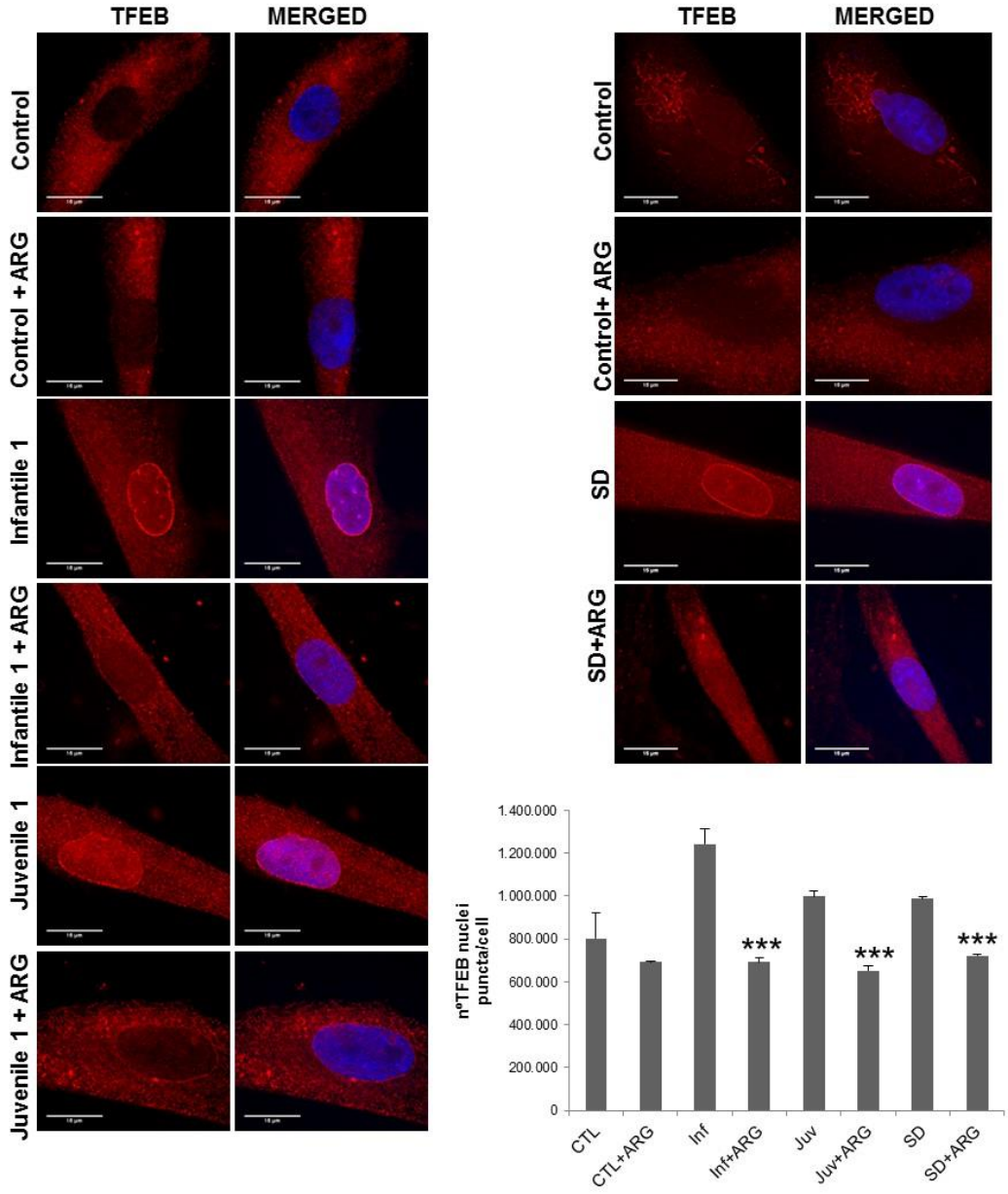

Supplementary Figure 14. Representative fluorescence images and quantification of fibroblasts from control, Tay-Sachs (infantil and juvenile) and Sandhoff (SD) with and without L-arginine treatment. Cells were fixed and stained with anti-TFEB antibodies (red). Nuclei were stained with Hoechst 33342 (blue). Increased TFEB in nucleus are shown in patients by red and blue fluorescence signal colocalization which was reduced after L-arginine treatment.